JOURNAL OF GEOPHYSICAL RESEARCH, VOL. 111, C12017, doi:10.1029/2005JC003247, 2006

Effects of the seasonal cycle on the development and termination of the Indian Ocean Zonal Dipole Mode

D. J. Halkides,[1] Weiqing Han,[1] and Peter J. Webster[2]

Received 24 August 2005; revised 22 April 2006; accepted 29 June 2006; published 22 December 2006.

[1] Effects of the seasonal cycles of atmospheric surface forcings on the development and termination of the Indian Ocean Zonal Dipole Mode (IOZDM) are studied using a nonlinear, 4-1/2 layer ocean model partially coupled to an advective atmospheric mixed layer model in which sea surface temperature (SST) feeds back only to air temperature and specific humidity. A series of experiments are performed for the period of 1984–1998 to isolate processes. The results indicate the seasonal cycle of atmospheric forcing aids development and decay of cold SST anomalies (SSTA) in the eastern basin associated with strong, positive dipole events. During the strong IOZDM years of 1994 and 1997, seasonal southeasterlies associated with the Asian summer monsoon reinforce coastal upwelling associated with the IOZDM near Sumatra-Java in boreal summer and fall, assisting initiation and increasing the peak amplitudes of these events. However, near the equator, fall equatorial westerlies deepen the thermocline in the eastern basin, reducing the cold SSTA in the eastern equatorial region and near Sumatra and Java. This contributes to the early termination of the 1994 IOZDM. In boreal winter the monsoon wind reversal reduces coastal upwelling along Sumatra and Java, further contributing to IOZDM termination. Moreover, the seasonal equatorial westerlies during fall and the monsoon wind reversal during winter counter southeasterly wind anomalies associated with the IOZDM in the eastern antinode region, reducing the total wind speed, weakening entrainment cooling and surface turbulent heat loss and thus further assisting IOZDM termination.

Citation: Halkides, D. J., W. Han, and P. J. Webster (2006), Effects of the seasonal cycle on the development and termination of the Indian Ocean Zonal Dipole Mode, *J. Geophys. Res.*, *111*, C12017, doi:10.1029/2005JC003247.

1. Introduction

1.1. Background

[2] The Indian Ocean Zonal Dipole Mode (IOZDM), also referred to as ''zonal mode'' or ''dipole mode,'' is a coupled ocean-atmosphere phenomenon in the tropical Indian Ocean (IO) that occurs on interannual timescales [e.g., *Saji et al.*, 1999; *Webster et al.*, 1999; *Yu and Rienecker*, 1999; *Murtugudde et al.*, 2000]. It has been directly linked to severe drought in Indonesia, excessive rainfall and flooding in Africa, and is hypothesized to be associated with the Asian-Australian monsoon [*Kapala et al.*, 1994; *Saji et al.*, 1999; *Clark et al.*, 2000; *Ashok et al.*, 2001; *Clark et al.*, 2003; *Loschnigg et al.*, 2003]. Positive IOZDM events are typically associated with cold SST anomalies (SSTA) in the southeastern tropical basin (10°S–EQ) and warm SSTA in the western tropics (Figure 1) [*Reverdin et al.*, 1986; *Saji et al.*, 1999; *Webster et al.*, 1999; *Murtugudde et al.*, 2000]. The situation reverses for negative IOZDM events. IOZDM strength is commonly measured by a dipole mode index (DMI) defined by *Saji et al.* [1999] as the difference in interannual SSTA between the tropical western (50°–70°E, 10°S–10°N) and southeastern IO (90°–110°E, 10°S–EQ; see boxed regions in Figure 1c); a ''strong event'' is defined to have a DMI exceeding 1 standard deviation.

[3] The onset, peak and termination periods of IOZDM events are phase-locked with the seasonal cycle [e.g., *Saji et al.*, 1999; *Webster et al.*, 1999]. Typically, a strong event begins concurrently with commencement of the Asian summer monsoon (Figures 1a and 1b), peaks during boreal fall (Figures 1c and 1d), and decays during the Asian winter monsoon (Figures 1e and 1f). At the time of onset, strong southeasterlies associated with the Asian summer monsoon along the coasts of Sumatra and Java shoal the thermocline and promote local, seasonal upwelling [*Susanto et al.*, 2001] (Figure 2a). The upwelling reaches a maximum in September (Figure 2b) when IOZDM events strengthen prior to their peaks. In the equatorial region, equatorial westerlies are enhanced during the transition between the summer and winter monsoons (Figure 3a), deepening the thermocline in the eastern equatorial basin during fall (Figure 3b). The deepened thermocline propagates southward along Sumatra-Java as coastal Kelvin waves [*Clarke and Liu*, 1993; *Wijffels and Meyers*, 2004], acting to reduce the seasonal upwelling along the coasts [*Susanto et al.*, 2001] (Figures 2c

[1]Department of Atmospheric and Oceanic Sciences, University of Colorado, Boulder, Colorado, USA.
[2]School of Earth and Atmospheric Sciences, Georgia Institute of Technology, Atlanta, Georgia, USA.

0148-0227/06/2005JC003247$09.00

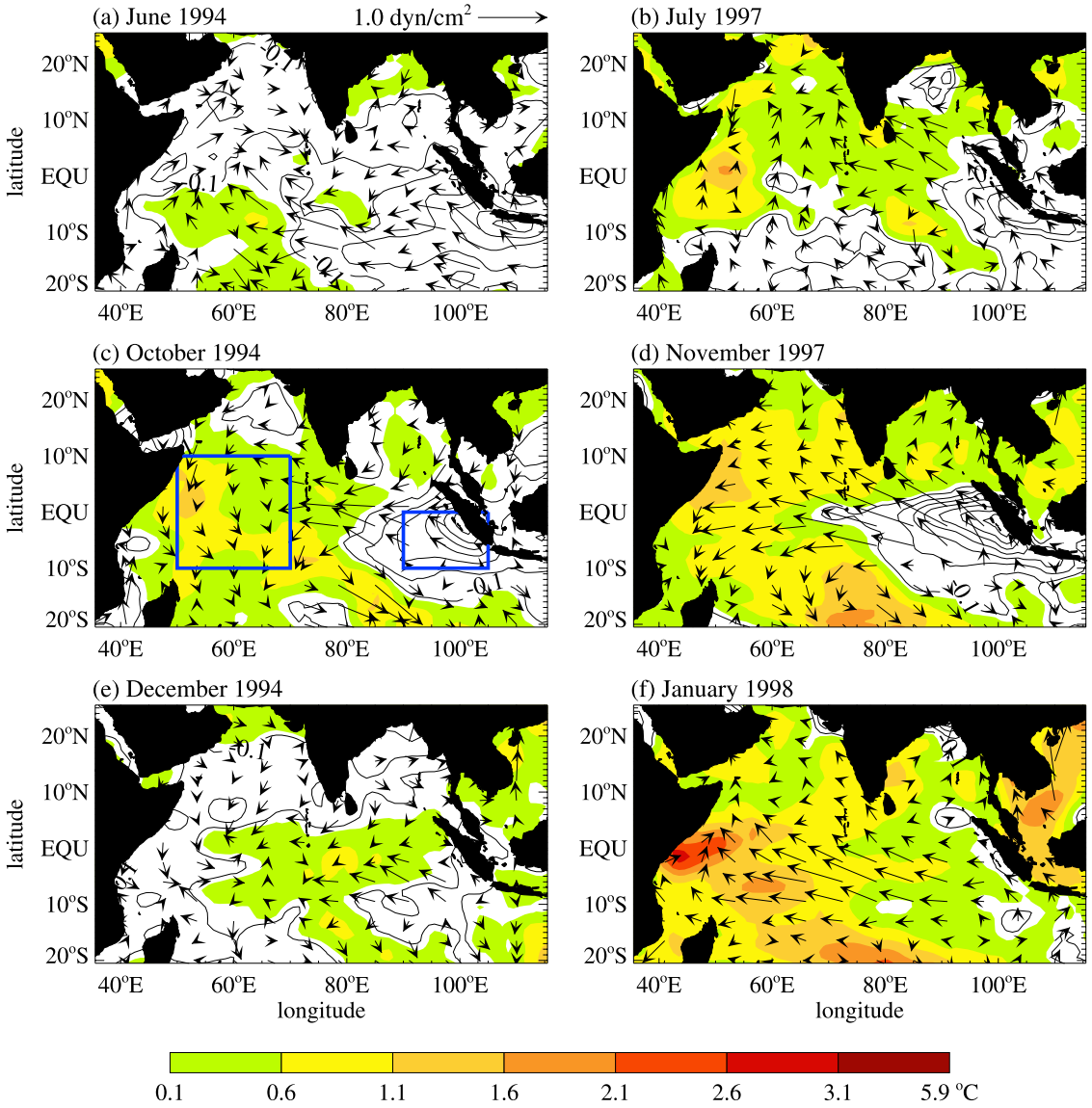

Figure 1. Observed interannual SSTA from *Smith and Reynolds* [2003] during select months of positive IOZDM years (left) 1994 and (right) 1997. Panels illustrate summer initiation, fall peak, and winter termination of these events. SSTA is defined as SST with the monthly mean climatology removed. Positive SSTA contours are colored; negative ones are shown as line contours of interval 0.5 °C; zero contours are suppressed. Vectors show observed interannual wind stress anomalies in dyn/cm^2 from Florida State University. Boxed regions in Figure 1c show the eastern and western IOZDM antinode regions defined by *Saji et al.* [1999].

and 2d). Note the deep thermocline in the eastern equatorial basin during both fall and late spring (Figure 3b) is associated with swift, eastward surface currents (Figure 3c), known as Wyrtki jets [*Wyrtki*, 1973], which are primarily driven by the seasonal winds [*Wyrtki*, 1973; *Jensen*, 1993; *Han et al.*, 1999], although they may consist of a series of intraseasonal jets [*Senan et al.*, 2003]. During winter, when IOZDM events decay, seasonal northwesterly monsoon winds near Sumatra-Java weaken the southeasterly trades, deepen the thermocline and cause coastal downwelling (compare the region just south of Java in Figures 2b and 2d).

[4] The temporal congruity of the seasonal cycle and IOZDM evolution indicates that seasonal circulations driven by the local monsoon winds may provide favorable conditions for, and thus play an important role in, IOZDM development and termination in the eastern antinode region. On the other hand, the strengthening of seasonal equatorial westerlies during summer–winter monsoon transitions in boreal fall tends to reduce coastal upwelling along Sumatra-Java and thus may weaken, or even contribute to the termination of, an IOZDM event. Hereafter, seasons refer to those of the northern hemisphere.

[5] A few existing studies have linked IOZDM termination to the seasonal cycle. *Annamalai et al.* [2003] suggested that seasonal variation of the southeasterly trade winds near Sumatra, which are weakened by the winter monsoon and thus reduce upwelling and evaporation, may

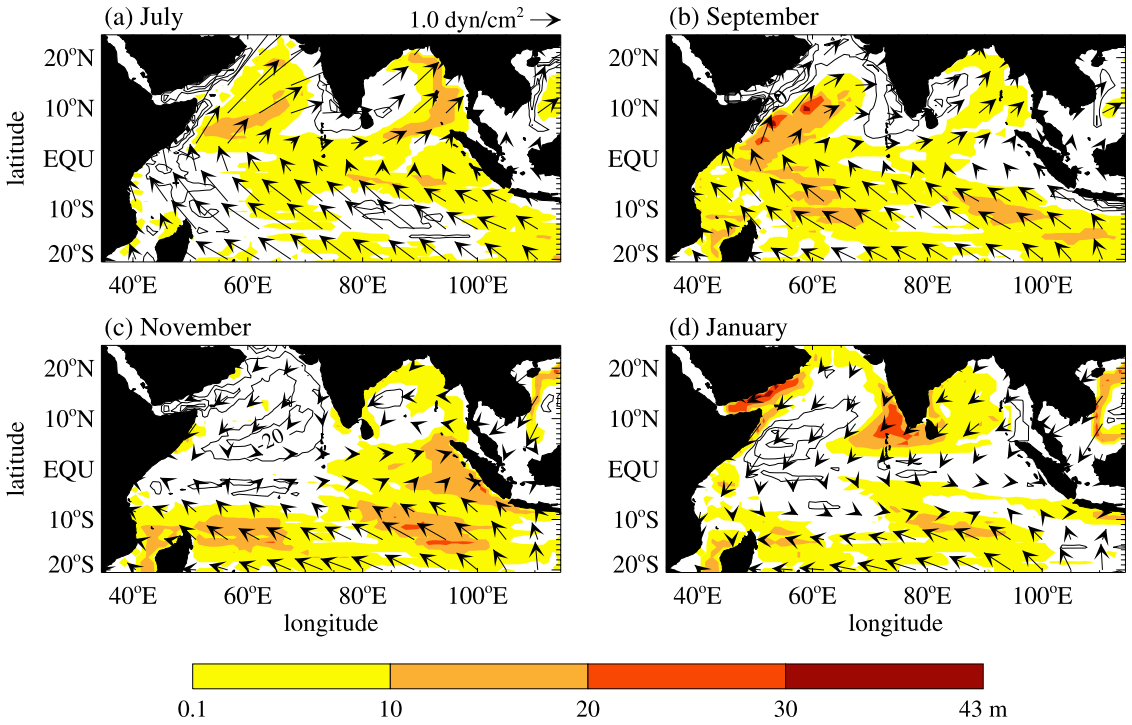

Figure 2. Seasonal cycle of SODA 20 °C isotherm depth as a proxy for thermocline depth: (a) July, (b) September, (c) November, and (d) January. Values above 0.1 m are colored; otherwise, line contours are used at an interval of 10 m. FSU climatological wind stress vectors are superimposed over depth contours with units of dyn/cm^2.

be a cause of IOZDM decay. *Murtugudde et al.* [2000] argued that surface warming caused primarily by reduced wind speed in the eastern basin during the fall may be accelerated in IOZDM years because of the thin surface mixed layer along Sumatra and thus may help the cold SST return to normal, a process demonstrating interaction between the seasonal cycle and interannual variability. *Saji et al.* [1999] proposed that austral summer insolation warming of the southeastern IO, also enhanced in IOZDM years by reduced convection over Indonesia and the thin mixed layer, may lead to decay of the eastern antinode. None of these studies, however, carefully isolated and explicitly examined

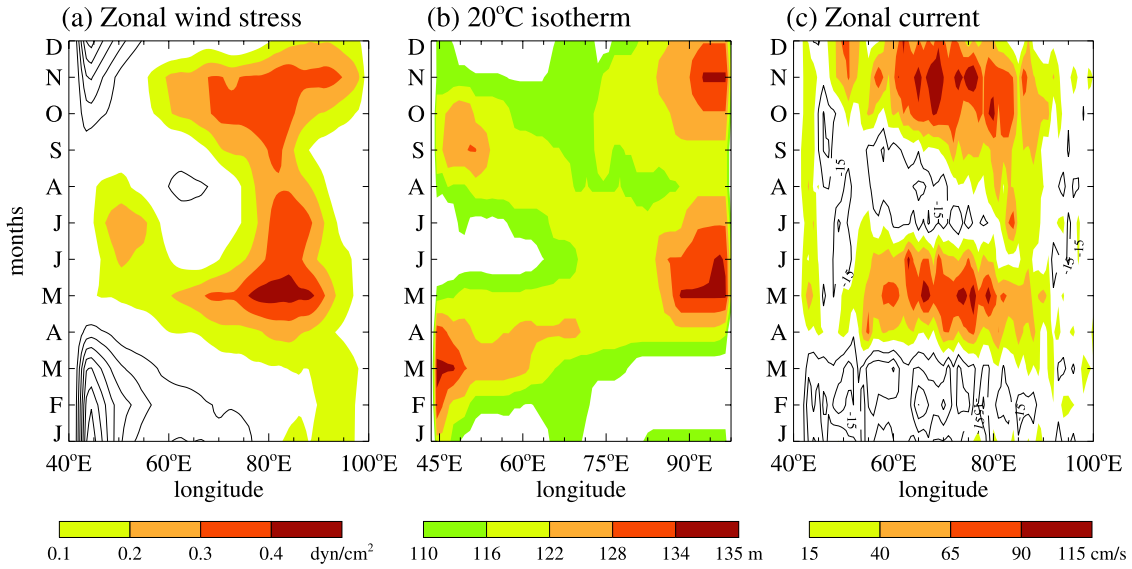

Figure 3. Climatologies along the Indian Ocean equator for (a) observed zonal FSU wind stress (1°S–1°N) in dyn/cm^2, (b) depth of the SODA 20 °C isotherm as a proxy for the depth of the middle of the thermocline (1.6°S–1.6°N) in meters, (c) ship drift zonal current at the surface, from *Mariano et al.* [1995] (1°S–1°N), in cm/s.

the effects the seasonal forcings of these proposed mechanisms have on the development and termination of IOZDM events. Furthermore, the likelihood that a deepened thermocline, caused by fall enhancement of equatorial westerlies, plays a significant role in IOZDM termination has neither been proposed nor tested in previous literature.

1.2. Present Research

[6] The goal of this paper is to provide a detailed examination of the role played by seasonal forcing in the initiation, development and termination of IOZDM events, for purposes of improving understanding of IOZDM phase locking with the seasonal cycle. To accomplish this goal, we performed a series of experiments using a 4-1/2 layer ocean model partially coupled to an advective atmospheric mixed layer (AML) model [*Seager et al.*, 1995; *Murtugudde et al.*, 1996]. This model (section 2) allows us to approximately isolate the primary processes through which seasonal atmospheric forcing is likely to affect the IOZDM, a difficult task with a fully coupled system. However, our model maintains the complexity required to achieve solutions that compare well to observations (section 2) [e.g., *Han et al.*, 2004].

[7] It is important to realize that the timing of IOZDM events has also been linked to both interannual and intraseasonal phenomena. For example, cross equatorial heat transport associated with the seasonally phase-locked Tropical Biennial Oscillation has been suggested to be a possible cause and regulator of the IOZDM [*Loschnigg et al.*, 2003]. Onset of El Niño in the Pacific, which tends to occur in June–July, can cause anomalous upwelling favorable winds along Sumatra-Java that sometimes trigger the IOZDM [*Annamalai et al.*, 2003]. The irregularity of IOZDM events has been partly attributed to intraseasonal atmospheric forcing [*Rao and Yamagata*, 2004; *Han et al.*, 2006]. *Han et al.* [2006], however, demonstrated that intraseasonal atmospheric forcing cannot explain the early termination of the eastern antinode in 1994, and suggested the seasonal cycle may play some role in the termination, listing *Halkides* [2005] as a reference. In this paper, we focus solely on understanding what roles seasonal atmospheric forcings play in modulating the IOZDM, particularly in the seasonal phase locking of events.

[8] The remainder of this paper is organized as follows. Section 2 describes the model and experiments. Section 3 validates the model and discusses the model results. Finally, section 4 provides a summary and concluding remarks.

2. Model

2.1. Ocean Model

[9] The ocean model is a nonlinear 4-1/2 layer system with active dynamics, thermodynamics and mixed layer physics. The model consists of four active layers that span roughly a few hundred meters of the upper ocean, overlying a deep inert layer where motion is assumed to vanish. Layer 1 represents the surface mixed layer, layer 2 is the seasonal thermocline, layer 3 is the thermocline and layer 4 is the upper intermediate water. The mixing scheme for the surface mixed layer is based on Kraus-Turner mixed layer physics [*Kraus and Turner*, 1967] and is also Richardson number-dependent. The thicknesses of layers 1 and 2, h_1 and h_2, are not permitted to become thinner than the minimum values $h_{1\min}$ = 10 *m* and $h_{2\min}$ = 10 m. These minima are necessary to keep the model numerically stable. However, these values are sufficiently small that solutions are not sensitive to them. Solar radiation penetration is based on the formula of *Morel and Antoine* [1994].

[10] This model has been applied to several Indian Ocean studies and produces realistic upper ocean circulations that compare favorably with observations [e.g., *Han et al.*, 1999; *Han and McCreary*, 2001; *Han and Webster*, 2002]. Both the upper ocean circulation and the heat transport produced by this model are as good as those from an ocean general circulation model (see *Han et al.* [2004] for the comparison). As the processes that affect the SST are discussed extensively in this paper, here we provide the equation for the mixed layer temperature. A detailed discussion of this model is given by *Han* [1999].

[11] The SST equation is

$$T_{1t} = -v_1 \cdot \nabla T_1 + \frac{Q_1}{h_1} + w_1^+ \frac{T_2 - T_1}{h_1} + \kappa_T \nabla^2 T_1 - \kappa_{T4} \nabla^4 T_1, \tag{1}$$

where T_1 and v_1 are mixed layer temperature and currents, Q_1 is the net heat flux for layer 1, w_1^+ is the rate of entrainment into the mixed layer, T_2 is layer 2 temperature, κ_T and κ_{T4} are harmonic and biharmonic mixing coefficients, respectively. The terms on the right side of equation (1) represent changes in mixed layer temperature with respect to time because of (1) horizontal advection; (2) net heat flux ($Q_1 = Q_{sw} - Q_{pen} + Q_{lw} + Q_{sen} + Q_{lat}$), which includes net solar heating (short wave radiation, Q_{sw}, at the surface minus its penetration, Q_{pen}, at the mixed layer bottom), long wave radiation (Q_{lw}), sensible and latent heat fluxes (Q_{sen} and Q_{lat}); (3) the transfer of heat between layers 1 and 2 via entrainment and upwelling; and (4) harmonic and (5) biharmonic horizontal mixing.

2.2. Atmospheric Mixed Layer Model

[12] The AML model has been described in detail by *Seager et al.* [1995; also see *Murtugudde et al.*, 1996]; thus here we only provide a brief discussion. The model represents the lowest 600 m of the planetary boundary layer. Within this layer, the air temperature and specific humidity are determined by a balance between surface fluxes (calculation of which requires the ocean model SST), horizontal advection by observed winds, entrainment from above, horizontal diffusion, and, for air temperature, radiative cooling. Air temperature and specific humidity from the AML, SST from the ocean model, and observed winds are then used to determine latent and sensible heat fluxes at the ocean surface. Additionally, observed cloud fraction is used to determine long wave heat flux. All three surface heat fluxes, as well as observed solar short wave radiation, are then used to determine the total heat flux, Q_1, acting on the mixed layer.

2.3. Boundary Conditions, Forcing, and Numerics

[13] The model basin resembles the real tropical IO (compare Figures 1 and 7) and includes the Maldive Islands. As our focus is to examine the effects of seasonal surface forcing on the IOZDM, the Indonesian Throughflow is not included.

[14] Wind stress used in both the ocean and atmosphere models was derived from Florida State University (FSU)

monthly mean pseudostress ($|V|V$) [*Legler et al.*, 1989]; rainfall was from the Climate Prediction Center Merged Analysis of Precipitation (CMAP); solar radiation data was from the International Satellite Cloud Climatology Project-Flux Data (ISCCP-FD) [*Zhang et al.*, 2004] and provided by Y. Zhang and W. Russow at NASA; scalar wind speed was created by adding climatological data from the Comprehensive Ocean-Atmosphere Data Set (COADS) to interannual anomalies from the National Centers for Environmental Prediction–National Center for Atmospheric Research (NCEP-NCAR) monthly mean reanalysis. (The decision to blend COADS climatologies with NCEP interannual anomalies was based on our preliminary runs, which showed that when the ocean is forced by NCEP data alone, corrective factors are required for the model to yield the most physically realistic SSTs. *Schiller and Godfrey* [2003] also blended NCEP and FSU wind stresses to improve their OGCM results. For this study, COADS climatology data plus NCEP anomalies are used for scalar wind speed, because FSU wind data only includes monthly pseudostress, not wind speed product. We have tested the monthly wind speed converted from monthly FSU wind stress, however, and the change is modest.)

[15] Model solutions were determined numerically on a staggered rectangular grid with 55 km × 55 km resolution; the AML model adapts directly to the ocean grid and it is assumed to be in equilibrium.

2.4. Interannual SSTA Induced by the Seasonal Cycle

[16] Seasonal forcing can induce interannual variability in SST through nonlinearities in the oceanic system. In equation (1), any variable can be expanded into mean, seasonal and interannual components, i.e., $T_1 = \bar{T}_1 + T_1^\star + T_1'$, where $\bar{T}_1$ is the long-term mean, $T_1^\star$ is the seasonal cycle and T_1' is the interannual variability. When equation (1) is expanded in this fashion, it is apparent that interannual SST variability cannot be fully separated from the seasonal cycle in this system. Below, we discuss the major nonlinear processes through which seasonal forcings can modify interannual SSTA, focusing on those processes that have a significant influence on IOZDM events, as shown later in sections 3.2 and 3.3.

2.4.1. Upwelling and Entrainment ($w_1^+\frac{T_2-T_1}{h_1}$)

[17] Seasonal wind stress, such as that associated with southeasterlies along the Sumatra and Java coasts during summer and fall, can cause coastal upwelling, shoal the thermocline and cause a thin $h_1^\star$. Since $h_1 = \bar{h}_1 + h_1^\star + h_1'$ is in the denominator of term 3 of equation (1), entrainment and upwelling cooling is nonlinear. A thin $h_1^\star$ can enhance interannual cooling via $w_1^+\frac{T_2-T_1}{h_1}$, reducing interannual SST. Meanwhile, seasonal upwelling of the colder thermocline water acts to decrease layer 2 temperature (T_2) and thus increase interannual cooling through its nonlinear relationship with $w_1^{+\prime}$ (or $w_1^{+\prime}\frac{T_2^\star-T_1^\star}{h_1}$). Physically, these processes indicate that a shallow thermocline caused by seasonal upwelling provides favorable conditions for enhancing the interannual cooling associated with the IOZDM in the eastern antinode region. The variable h_1' (which is modified by seasonal wind stress in the model partly via seasonal advection of h_1', and interannual advection of $h_1^\star$) can also affect interannual SSTA through the mechanisms described above. Furthermore, because the entrainment rate (w_1^+) is proportional to the wind speed cubed rather than the wind speed itself, a change in total wind speed due to the seasonal cycle can induce changes in $w_1^{+\prime}$ and thus cause interannual variability of entrainment cooling, affecting interannual SSTA.

2.4.2. Surface Heating $\left(\frac{Q_1}{h_1} = \frac{Q_{sw}-Q_{pen}+Q_{lw}+Q_{sen}+Q_{lat}}{h_1}\right)$

[18] Since both Q_{sen} and Q_{lat} depend on wind speed and SST in a nonlinear manner [*McCreary and Kundu*, 1989], changes in seasonal wind speed can alter interannual SSTA by causing interannual anomalies of latent and sensible heat fluxes, Q'_{lat} and Q'_{sen}. This effect is enhanced when h_1 is thin. All seasonal heating processes, such as seasonal insolation ($Q_{sw}^\star$), can cause interannual SST anomalies because of the presence of $h_1 = \bar{h}_1 + h_1^\star + h_1'$ in the denominator of the surface heating term, since h'_1 can cause interannual variability in, for example, $\frac{Q_{sw}^\star}{h_1}$. Additionally, interannual variability of h_1 also affects Q_{pen}, further modifying the effects of seasonal solar heating.

2.4.3. Horizontal Advection ($-\boldsymbol{v_1}\cdot\boldsymbol{\nabla T_1}$)

[19] The seasonal cycle can also cause interannual SSTA via the following terms: $-v_1^\star\cdot\nabla T_1' - v_1'\cdot\nabla T_1^\star - v_1'\cdot\nabla T_1'$. Respectively, these represent advection of interannual SSTA by seasonal currents, advection of seasonal SSTA by interannual currents, and advection of interannual SSTA by interannual currents.

[20] The complexity of these nonlinear interactions makes a complete isolation of the effects of the seasonal cycle impossible. However, we can isolate the interannual SSTA caused by the seasonal cycles of atmospheric forcing fields numerically, then identify the processes involved with the aid of the above mentioned nonlinear mechanisms.

2.5. Experiments

[21] A series of model experiments was performed (Table 1), in order to estimate effects of the seasonal cycles of surface forcings on the IOZDM. All experiments were performed for the 15 year period of January 1984 to December 1998, a period for which all forcing fields were available, and that includes both two strong positive IOZDM events in 1994 and 1997, and two weak events (with peak DMI magnitudes between 1 and 0.5 DMI standard deviations) in 1987 and 1991 [*Annamalai et al.*, 2003; *Shinoda and Han*, 2005]. In this paper, we focus specifically on the strong 1994 and 1997 events. Discussion of additional events, including the negative dipoles of 1996 and 1998, is given by *Halkides* [2005].

2.5.1. Main Run (MR)

[22] The MR was forced by the interannually varying monthly fields described in section 2.3. It provides a realistic simulation of both the seasonal cycle and interannual variability in our regions of interest. In accordance with section 2.4, the seasonal cycle is defined as the monthly climatology with the long-term mean for the period of interest removed. Interannual variability is the deviation from the monthly climatology, a definition that follows convention. The test runs (TR) described below are designed to isolate the effects of specific seasonal forcings and their associated processes.

2.5.2. TR0, All Seasonal Forcing Removed

[23] In TR0, the seasonal cycle was removed from all monthly forcing fields for the period of 1984–1998. For each field, this was achieved by subtracting the seasonal

Table 1. Series of Experiments Used to Isolate Effects of Specific Physical Processes on Interannual IO SSTA[a]

Run Name	Description
MR	Main Run, forced by complete monthly forcing
TR0	no seasonal forcing
TR1	seasonal wind stress removed
TR2	seasonal wind speed removed from the ocean entrainment cooling calculations
TR3	seasonal wind speed removed from AML surface heat flux calculations
TR4	seasonal insolation cycle removed from short wave heat flux at the surface

[a]All runs were forced with data for January 1984 to December 1998.

cycle from monthly data of each year at each grid point. Interannual SSTA from the difference solution (MR−TR0) estimates the response to total seasonal forcing. This paper focuses on examining the SSTA responses associated with the IOZDM.

2.5.3. TR1, Seasonal Wind Stress Forcing Removed

[24] In TR1, the seasonal cycle was removed from the wind stress forcing only. Otherwise, TR1 is identical to the MR. Interannual SSTA from the difference solution (MR−TR1) measures the effects of seasonal wind stress forcing. This experiment will test the hypotheses that changes in coastal upwelling due to the local monsoon reversals along the Sumatra-Java coasts play an important role in IOZDM phase locking, and that the semiannual equatorial zonal winds, in particular the westerlies during fall, can have a significant influence on IOZDM termination in the eastern antinode region.

2.5.4. TR2, Seasonal Wind Forcing of Entrainment Cooling Removed

[25] In TR2, the seasonal cycle was removed from the wind speed field used solely to calculate vertical entrainment into the oceanic mixed layer. Otherwise, it is the same as the MR. The difference between the MR and TR2 estimates the effects of the seasonal winds on the IOZDM through modulation of entrainment cooling.

2.5.5. TR3, Seasonal Wind Forcing of Surface Turbulent Heat Flux Removed

[26] In TR3, the seasonal cycle was removed from the wind speeds used to calculate latent and sensible heat flux in the AML model. TR3 is otherwise identical to the MR. The difference solution (MR−TR3) estimates the effects of seasonal winds on the IOZDM through changing latent and sensible heat fluxes. This will test the hypothesis that the winter monsoon wind reversal, which reduces local wind speed, contributes to termination of the eastern IOZDM antinode.

2.5.6. TR4, Seasonal Insolation Removed

[27] In TR4, the seasonal cycle was removed from the incoming solar radiation only. The difference between the MR and TR4 solutions yields the response to seasonal insolation, which increases in the southern tropical basin during the time of IOZDM termination.

[28] An additional experiment was performed to isolate the effects of the seasonal cycle of cloud fraction on outgoing long wave radiation at the surface. The resulting effect, however, is negligible and thus will not be discussed.

3. Results

[29] In this section, we first examine the model performance to demonstrate its suitability for our purposes. Then, we examine the series of experiments to estimate the effects of seasonal surface forcing on the IOZDM, focusing on the strong 1994 and 1997 events. Although these two events bear many similarities, they also exhibit significant differences. For example, the 1994 event has an early peak and rapid termination, whereas the 1997 event is extremely strong and has a late peak and prolonged duration [e.g., *Han et al.*, 2006] (Figure 1). These differences may result partly from contributions of the seasonal cycle through nonlinearity in the system. Additionally, while the western antinode is an important part of the IOZDM that can affect dipole strength through Bjerknes feedback, recent work suggests the eastern antinode is crucial for IOZDM initiation; for example, the latter can be triggered by remote forcing associated with ENSO events in the Pacific [*Annamalai et al.*, 2003]. In our model, the most significant SSTA responses to seasonal forcing are also in the eastern IO during positive dipole events. Thus we will focus largely on the eastern antinode region and will discuss the western antinode region only when the seasonal cycle has a large influence there.

3.1. Model Validation

[30] Seasonal variations of the circulation, mixed layer and SST in the upper tropical IO have been studied extensively over the past two decades [e.g., *Luther and O'Brien*, 1985; *Reverdin*, 1987; *Kindle and Thompson*, 1989; *McCreary et al.*, 1993; *Murtugudde et al.*, 1996; *Rao and Sivakumar*, 2000; *Schott and McCreary*, 2001, and references therein; *Maghanani et al.*, 2003]. Here, we compare the seasonal cycle in the MR solution to observations, focusing specifically on aspects of the seasonal cycle that are relevant to this paper.

[31] Figure 4 shows the seasonal cycles of MR SST (solid lines), averaged over the western (50°−70°E, 10°S−10°N) and eastern (90°−110°E, 10°S−EQ) IOZDM antinode regions. The MR solution agrees favorably with observations (dash-dotted lines) in both antinode regions. This degree of agreement is comparable with, if not better than, existing model studies. There are, however, some quantitative model/data differences especially in the western antinode, where the peak amplitude of the simulated seasonal cycle is exaggerated a few tenths of a °C. These differences may result from inaccuracies in the forcing fields and from deficiencies in the model. Although significant, the error is sufficiently smaller than the signal amplitude that it should not have a significant influence on our results. Additionally, our discussion focuses on the eastern antinode region where errors are small. The spatial distribution of the SST climatology (not shown) also agrees well with observations [*Halkides*, 2005], as does seasonal variability of the thermocline and the equatorial surface currents. Comparing Figure 3b, which shows the seasonal cycle of 20 °C isotherm

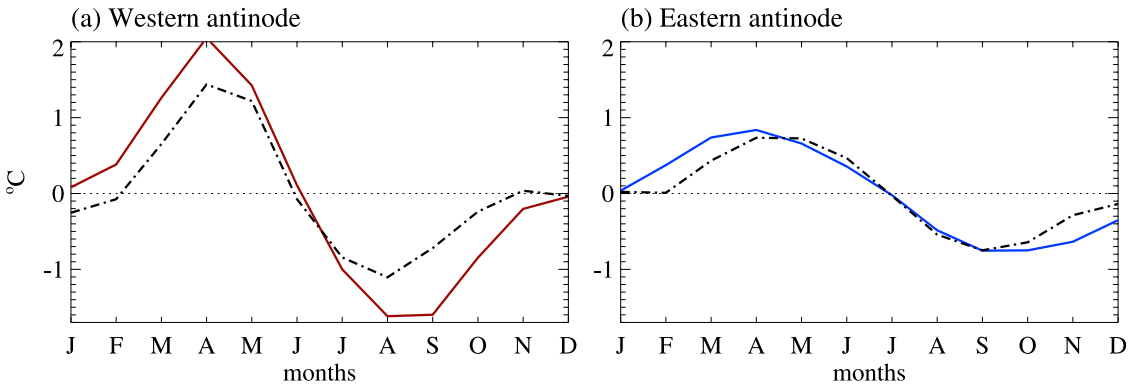

Figure 4. Seasonal cycles of the simulated MR (solid) and observed (dashed) SST in the (a) western (50°–70°E, 10°S–10°N) and (b) eastern (90°–110°E, 10°S–EQ) IOZDM antinode regions, in °C. Observed SST is from *Smith and Reynolds* [2003].

depth from the Simple Ocean Data Assimilation analysis (SODA) [*Carton et al.*, 2000] as a proxy for the depth of the central thermocline, and Figure 5a, which shows depth of the top of the thermocline in our model, we can see that the model reasonably simulates the thermocline deepening in the eastern equatorial basin during spring and fall. The model also reasonably reproduces the spring and fall Wyrtki jets, although throughout the year the simulated equatorial currents (Figure 5b) are weaker than the observed ones shown here (Figure 3c) for a couple of reasons. First, the simulated currents are an average for the entire depth of the mixed layer, whereas the ship drift data provides surface velocities. Also, the ship drift climatology was not based on data collected during the exact same period as our simulation [*Mariano et al.*, 1995], such that some quantitative differences between the data and model solution are expected. In particular, the ship drift data did not include 1997–1998, a strong IOZDM period when the fall Wyrtki jet almost disappeared [*Murtugudde et al.*, 2000]. Thus the weaker fall Wyrtki jet in the model seasonal cycle is not surprising. In addition, the monthly forcings do not include intraseasonal variability, which can affect the Wyrtki jet strength [*Senan et al.*, 2003] by about 10–15% [*Han et al.*, 2004].

[32] On interannual timescales, the strong IOZDM events in 1994 and 1997, and weak events in 1987 and 1991 are all reasonably simulated (Figure 6; compare Figures 7 (left) and 10 (left) with Figure 1 for spatial patterns). During these events, anomalous southeasterly winds in the eastern tropical basin shoal the thermocline and cause coastal and

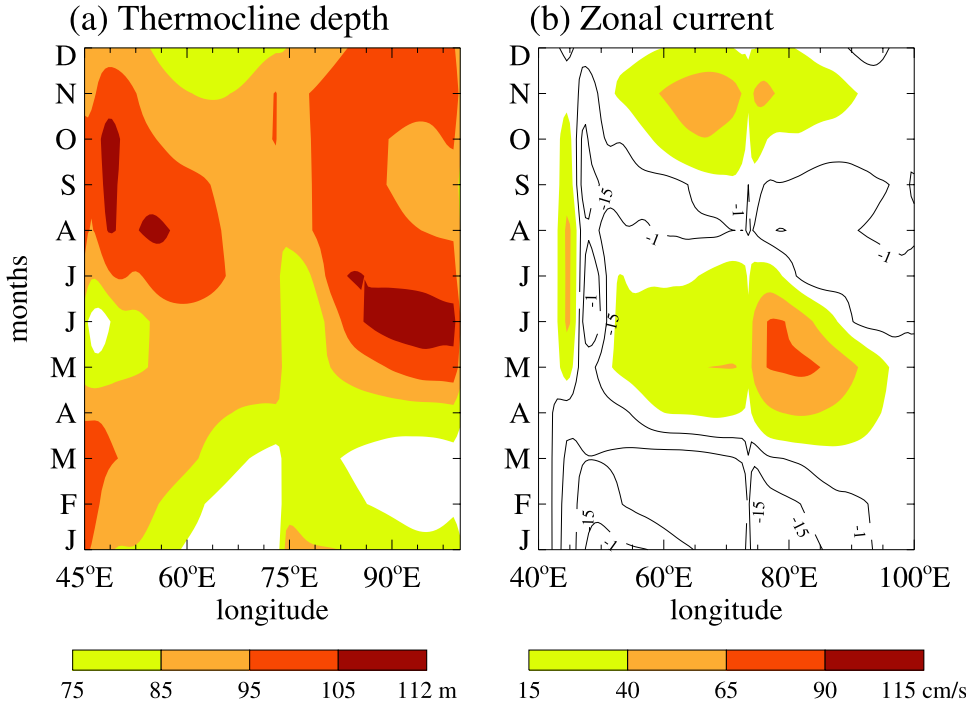

Figure 5. Simulated climatologies along the Indian Ocean equator from the MR for (a) the depth at the top of the thermocline ($h_1 + h_2$) in meters and (b) the zonal current in layer 1 (or the zonal current averaged over the depth of the mixed layer) in cm/s. Both quantities are averaged over 1°S–1°N.

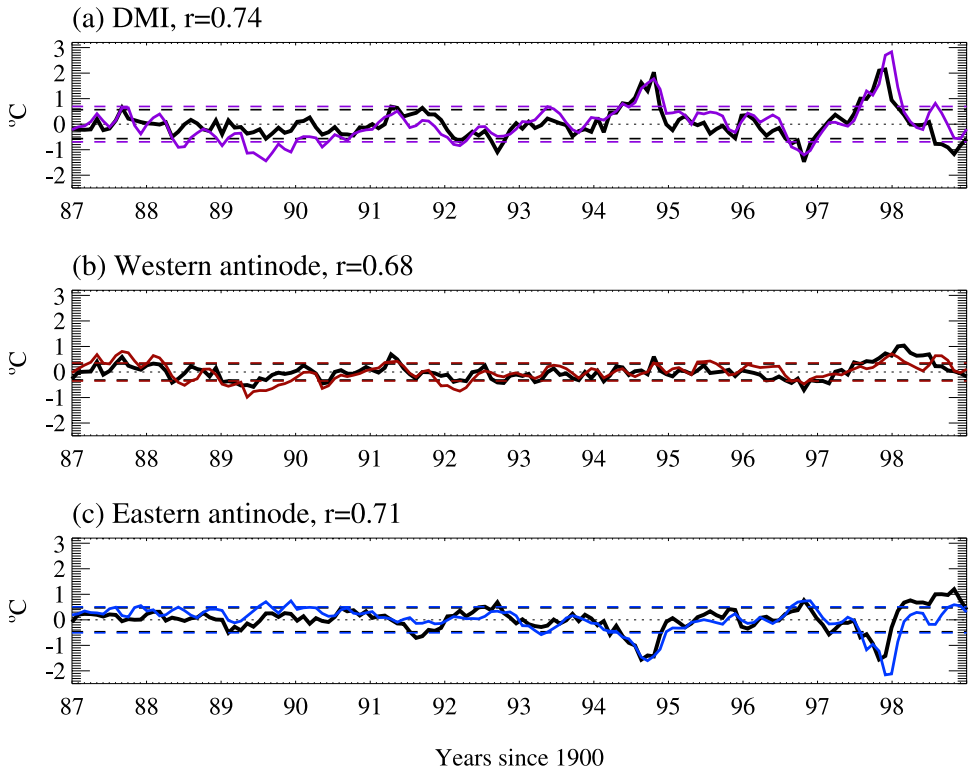

Figure 6. (a) Monthly DMIs calculated from MR interannual SSTA (in color) and observed *Smith and Reynolds* [2003] SSTA (in black), (b) western IOZDM antinode SSTA indices, and (c) eastern antinode indices. Units are °C. In all three panels, dashed lines denote the standard deviation above and below the mean for each index. Correlation coefficients (r) for simulated and observed indices appear above each panel.

equatorial upwelling, producing the cold SSTA in the eastern antinode region [*Reverdin et al.*, 1986; *Saji et al.*, 1999; *Webster et al.*, 1999; *Murtugudde et al.*, 2000]. Concurrently, the equatorial easterly wind anomalies cause Ekman convergence off the equator and push the thermocline downward. The downward thermocline signals propagate westward as Rossby waves, deepening the thermocline and producing warm SSTA in the western antinode region [*Saji et al.*, 1999; *Webster et al.*, 1999; *Chambers et al.*, 1999; *Murtugudde et al.*, 2000]. The deepened thermocline associated with the western IOZDM antinode overlaps with the open ocean upwelling region near 2°–10°S [*McCreary et al.*, 1993; *Murtugudde et al.*, 1999; *Xie et al.*, 2002], where SST is particularly sensitive to changes in thermocline depth.

[33] Variability of the dipole mode strength (Figure 6a), and of interannual SSTA in the western and eastern antinode regions (Figures 6b and 6c) are reasonably simulated for 1994 and 1997/1998, as well as for 1987 and 1991. The correlation coefficients between the observed and simulated DMIs, western antinode SSTA, and eastern antinode SSTA are 0.74, 0.68, and 0.71, respectively, for the period of 1987–1998. This time range was chosen to exclude transient effects in the first 3 years of the model solution. Over January 1994 to December 1997, our period of interest, $r = 0.84$ in the eastern basin. This degree of similarity to data is good relative to comparable model studies. Further model/data consistency for the 1994 and 1997 IOZDM events will be given in the next section. Visual comparison indicates small phase discrepancies and a slightly smoother-than-observed simulated solution partly account for the difference indicated in the correlation values.

[34] Last, Figure 6c shows cold SSTA in the simulated eastern antinode during 1997/1998 is exaggerated in comparison to observations. *Halkides* [2005] showed that when observed air temperature and specific humidity are used to force the ocean model (no air-sea coupling), the simulated 1997 event is more similar to the observed event. This suggests that while the partially coupled model is more physically reasonable (in that air temperature and specific humidity are determined by SST in the tropical ocean rather than the other way around), adding this feedback can introduce error to the system because of inaccuracies in the coupled processes. Note that the 1997 eastern antinode is still slightly exaggerated in the fully forced version of the model [*Halkides*, 2005]; thus error in the model forcings may also contribute. It is possible that the increased error in 1997 stems from enhanced SST sensitivity to forcing in the eastern basin due to the unusually shallow thermocline there during this event. The fact that the simulated 1997 eastern antinode is colder than the observed during its peak may be responsible for the additional prolonging of the simulated event. Termination in this context is defined as the month in which the eastern antinode magnitude drops below 1 standard deviation. As this study is mostly concerned with SSTA responses to seasonal forcing, this is unlikely to qualitatively alter our results, and, as the difference between the observed

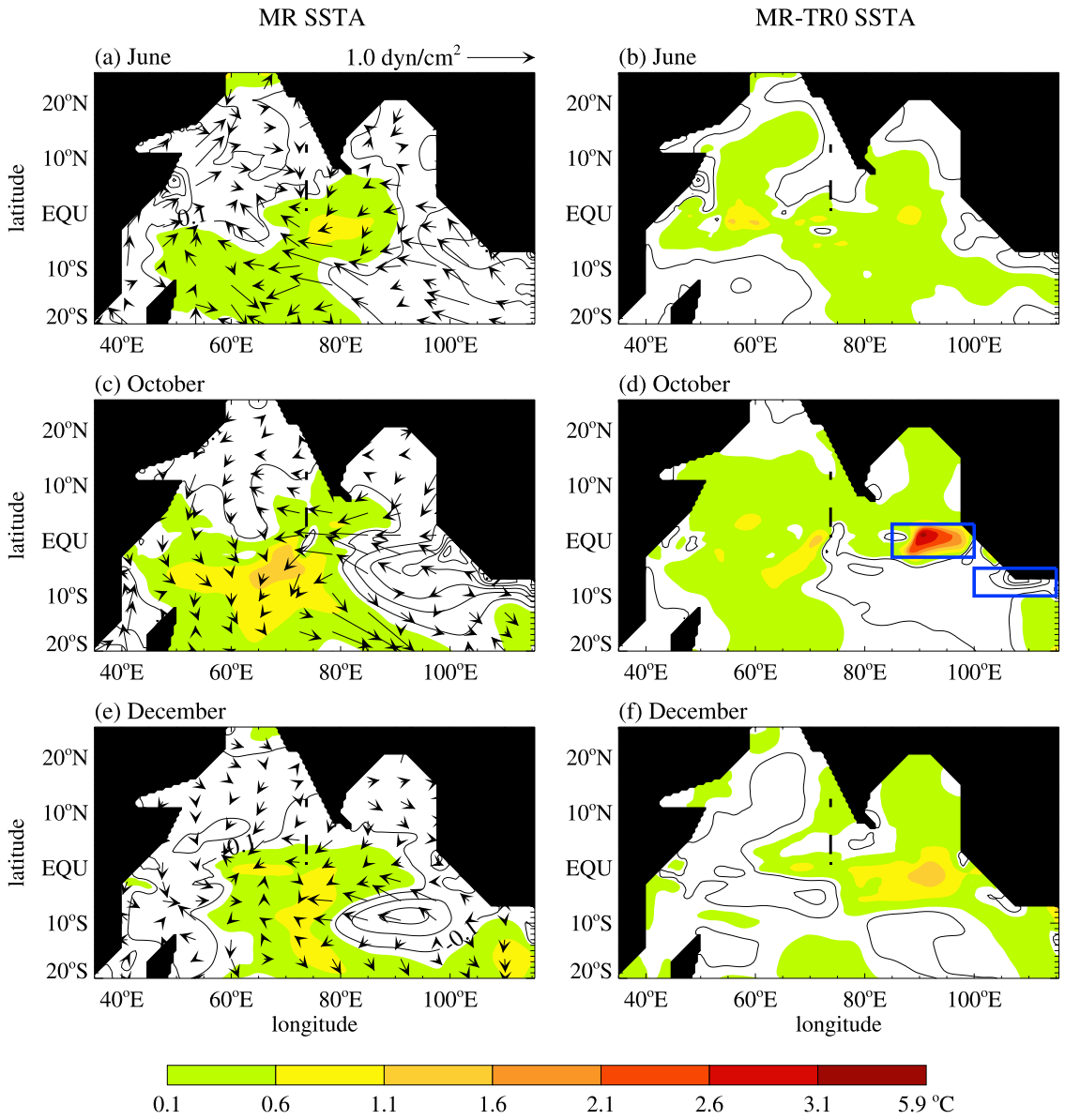

Figure 7. (left) Interannual MR SSTA with interannual FSU wind stress anomalies superimposed over the contours and (right) MR minus TR0 SSTA, for select months during the 1994 IOZDM. Positive anomalies are colored; negative anomalies are shown with line contours at an interval of 0.5 °C. Difference panels in right-hand column show the interannual SSTA response to total seasonal atmospheric forcing. (d) Boxes denote important responses within the eastern antinode along the equator (85°–100°E; 2°S–3°N) and in the southern Sumatra-Java upwelling region (100°–115°E; 5°–10°S).

and simulated signals is notably smaller than the amplitudes of those signals, quantitative effects should be minimal.

[35] The reasonable agreement between the model solution and observations on both seasonal and interannual timescales demonstrates this model is suitable for testing how interannual SSTA may respond to seasonal forcings and thus serves the purpose of this study.

3.2. Effects of the Seasonal Cycle on the 1994 IOZDM

[36] The strong 1994 IOZDM (Figure 1 (left)), reached peak magnitude in October and decayed rapidly thereafter. This was reasonably simulated by our model (Figure 7 (left)). Before examining the processes that contribute to seasonal modulation of this event in our model, we analyze the response of interannual SSTA to total seasonal atmospheric forcing during the 1994 event period.

3.2.1. SSTA Response to Total Seasonal Forcing

[37] Figure 7 shows interannual SSTA from solution MR (left column) and from the difference solution MR–TR0 (right column) during the 1994 IOZDM period. Recall that for TR0, the seasonal cycle was removed from all forcing fields and thus the MR–TR0 solution estimates the effects of total seasonal forcing. The most significant responses occur in the eastern equatorial basin and along the coasts of

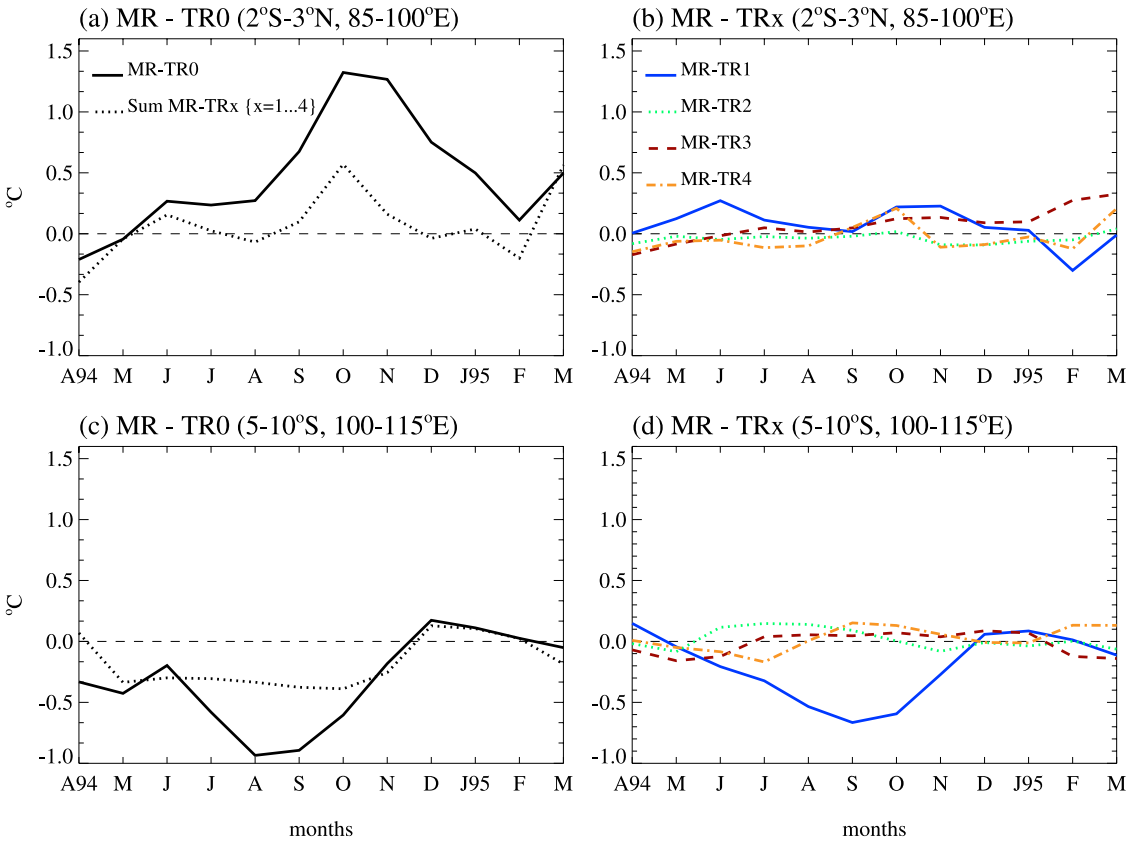

Figure 8. The mean SSTA responses (MR-TRx) (left) to total seasonal forcing and (right) to isolated seasonal forcings from April 1994 through March 1995 in two subregions of the eastern antinode: along the equator (2°S–3°N, 85°–100°E) and in the southern Sumatra-Java upwelling region (5°–10°S, 100°–115°E). Figures 8a and 8c include the summation of the isolated responses for comparison to the MR-TR0 indices. Index boxes are shown in Figure 7d.

southern Sumatra and Java, within the boxed areas in Figure 7d. To better quantify these responses, the time evolution of the MR–TR0 SSTA in each of these boxed regions during April 1994 to March 1995 is displayed in Figures 8a and 8c. Positive values indicate warming of SSTA by seasonal forcing; negative values denote cooling.

[38] In the eastern antinode region, seasonal surface forcing notably enhances the cold SSTA along the coasts of Sumatra and Java starting in June (Figures 7a and 7b). This cooling persists near the Java coast (southern box in Figure 7d) until the October event peak, helping to initiate the IOZDM (Figures 7c and 7d). On the other hand, in the eastern equatorial basin (equatorial box in Figure 7d), significant warming occurs in October–November (Figure 8a), which considerably weakens the negative SSTA associated with the IOZDM in this region (Figures 7c and 7d). This warming spreads southward in November–December (Figure 7f; compare Figures 8a and 8c), acting to bring the negative SSTA to normal. These results suggest that seasonal surface forcings may play an important role in causing the early termination of the 1994 IOZDM event.

[39] In the western basin, the seasonal cycle tends to enhance warm SSTA during the October 1994 IOZDM peak (Figures 7c and 7d), but subsequently, seasonal forcing spurs cooling of western SSTA (Figures 7e and 7f). Thus seasonal forcing also contributes to IOZDM termination in the western antinode region.

[40] Relative contributions of seasonal wind stress, wind speed and insolation to interannual SSTA in the eastern equatorial basin (2°S–3°N, 85°–100°E) and near the coasts of southern Sumatra and Java (5°–10°S, 100°–115°E) during the 1994 IOZDM are shown in Figures 8b and 8d, respectively. Solid lines show the interannual SSTA caused by seasonal wind stress (MR-TR1); dotted lines measure effects of entrainment induced by seasonal wind speed (MR-TR2); dashed lines estimate effects of turbulent heat fluxes caused by seasonal wind speed (MR-TR3); and dash-dotted lines show effects of seasonal insolation (MR-TR4). Note that adding the individual contributions together is qualitatively similar to, but does not quantitatively yield, the MR-TR0 SSTA caused by the total seasonal forcing in either region (see dotted lines in Figures 8a and 8c). This difference results from nonlinear interactions between processes (discussed in detail in section 2.4). Nevertheless, variations in the MR-TR0 SSTA bear a close resemblance to those in the sum of the individual processes, and the degree of similarity is quantitatively better for the 1997 event (see section 3.3). Note that the seasonal cycles of rainfall and cloud fraction have negligible influences, and thus their individual contributions are not shown.

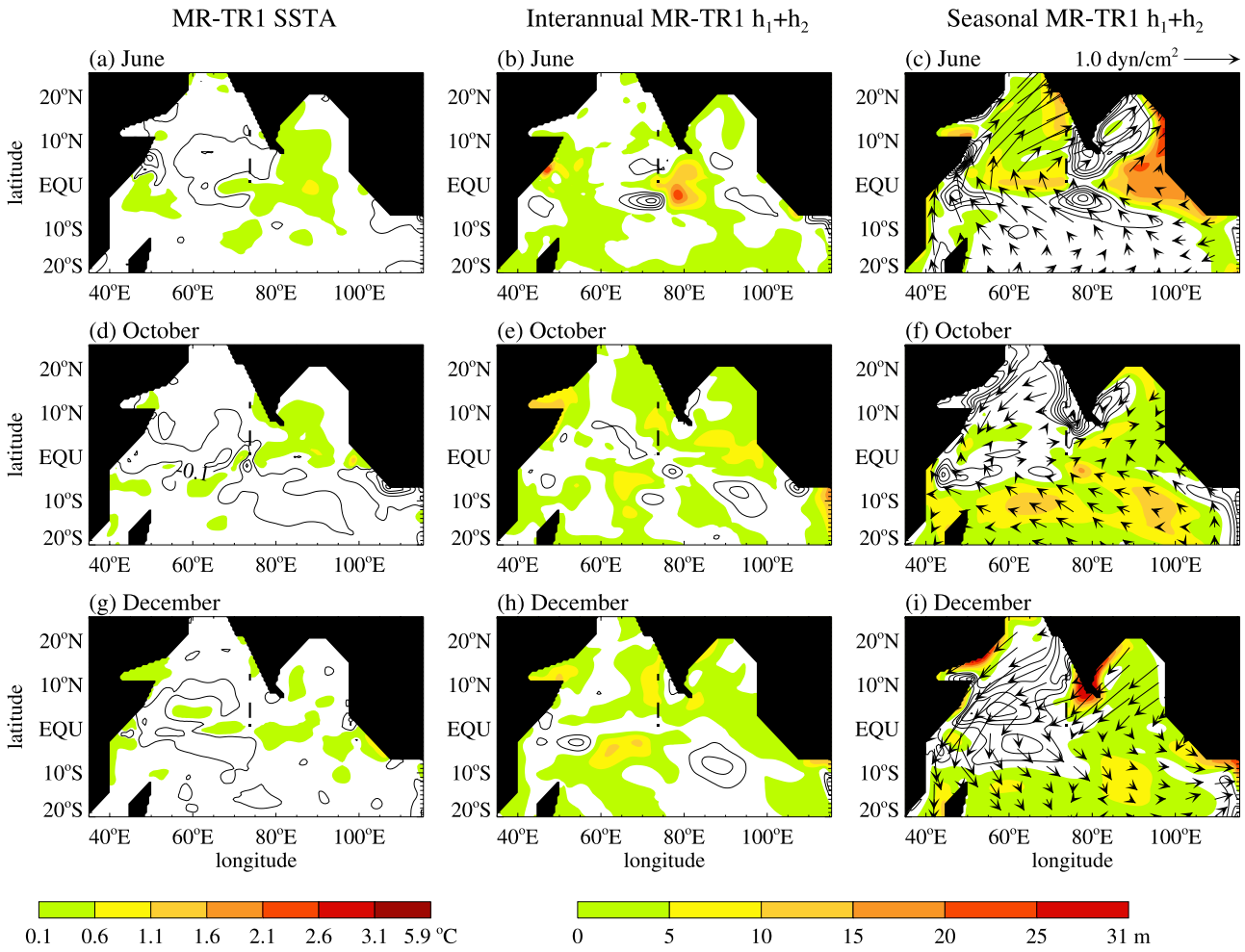

Figure 9. (left) Interannual MR minus TR1 SSTA for select months during the 1994 IOZDM. This represents the effect of seasonal wind stress on interannual SSTA variability. (middle) Interannual MR minus TR1 thermocline depth in meters. (right) Seasonal cycle of MR minus TR1 thermocline depth. Vectors show seasonal FSU wind stress in dyn/cm^2, the signal that was removed from the TR1 forcing. Positive anomalies are colored; negative anomalies are shown with line contours.

[41] Comparison of Figures 8c and 8d demonstrates that the effects of total seasonal forcing in the southern part of the eastern antinode result largely from seasonal wind stress. In the eastern equatorial region, variability of the SSTA response to total seasonal forcing (Figure 8a) also corresponds most closely to variability in the SSTA response to seasonal wind stress. Given the significance of wind stress to SSTA variability in both subregions, and more importantly, given the clear dominance of the seasonal wind stress effect near southern Sumatra and Java (Figures 8c and 8d), below, only the system response to seasonal wind stress is discussed in detail, with emphasis on the southern Sumatra-Java region.

3.2.2. SSTA Response to Seasonal Wind Stress

[42] The left column of Figure 9 shows the MR−TR1 interannual SSTA during the 1994 IOZDM period. This difference solution isolates the interannual SSTA response to seasonal wind stress (vectors in Figure 9 (right)), which affects SST in our model primarily through modulation of thermocline depth via Ekman divergence (upwelling) and convergence (downwelling), as well as advection. As discussed in section 2.4, seasonal wind stress can cause interannual SSTA variability via nonlinearities in these processes, which in equation (1) are associated with both $h_1^{\star}$ and h_1'. As h_1 and h_2 are closely related, the middle and right columns of Figure 9 show the interannual anomaly and seasonal cycle, respectively, of the MR−TR1 top of thermocline depth ($h_1 + h_2$). Vectors in the right column represent the seasonal cycle of the observed FSU wind stress, the signal that was removed from TR1. Note this differs from the observed wind stress climatology in Figure 2, which retains the long-term mean.

[43] The 1994 eastern antinode begins to develop in June (Figures 1 and 7), when seasonal southeasterlies associated with the Asian summer monsoon commence near Java (vectors in Figure 9c and Figure 2). These upwelling favorable monsoon winds cause a negative interannual thermocline anomaly near southern Java of over 5 m (Figure 9b) and thins our model h_1' (not shown). The thinner h_1' reduces h_1 (see section 2.4) and thus enhances upwelling cooling through the term $w_1^{+}\frac{T_2-T_1}{h_1}$ in equation (1). This process appears to contribute to the negative SSTA

near southern Sumatra and Java (Figure 9a), which strengthens initiation of the IOZDM (Figure 7a). The negative SSTA can feedback to the atmosphere to reduce air temperature and specific humidity, which can be further advected westward by the southeasterly winds associated with the IOZDM, cooling the SST in a larger region.

[44] The interannual thermocline anomaly near Java shown in Figure 9b may result from the westward seasonal South Equatorial Current (not shown) advecting the shallow interannual thermocline associated with the IOZDM, and from the northwestward interannual current [*Murtugudde et al.*, 2000] advecting the seasonal shoaling of the thermocline near southeast Java. In fact, the importance of advection for IOZDM development has been suggested by *Murtugudde et al.* [2000]. Note that while the response of SSTA to seasonal wind stress is small in June relative to that in October, the IOZDM signal is also weak during this time (also see Figures 7a and 7b). The seasonal cycle of thermocline variability caused by seasonal wind stress shows deepening in the eastern equatorial basin and along the coasts of Sumatra-Java during summer (Figure 9c); thus it is not likely contributing to IOZDM initiation. This deep thermocline is generated by the seasonal equatorial westerlies during April–May (Figure 3a), which cause equatorial convergence, push the thermocline downward, and instigate the spring Wyrtki jet [*Wyrtki*, 1973] (Figures 3 and 5). The deepened thermocline signals propagate poleward along the coasts of Sumatra-Java as coastal Kelvin waves (Figure 9c).

[45] From summer to early fall, the southeasterly monsoon winds are strong relative to those during the rest of the year (Figures 2 and 9 (right)). These relatively strong alongshore winds enhance coastal upwelling near Java and Sumatra, and produce a negative anomaly in the seasonal cycle of the thermocline south of Java during fall (compare Figures 9c and 9f). The shoaled thermocline enhances upwelling cooling and thus strengthens the eastern antinode during the event peak (Figure 9d). This result suggests the seasonal cycle of wind stress increases the peak magnitude of the 1994 IOZDM. In October, the interannual thermocline anomaly induced by seasonal wind stress is negative only at the southwestern tip of Sumatra (Figure 9e), however, this may also enhance cooling near that location.

[46] At the equator, the equatorial westerlies intensify again during October–November (Figure 3a). These westerly winds deepen the equatorial thermocline producing a positive anomaly in its seasonal cycle (Figures 9f, 3b, and 5a). Subsequently, this deep equatorial thermocline signal travels south along the coasts of Sumatra-Java via coastal Kelvin waves (Figure 9i). In December, this deepening of the seasonal signal is reinforced by northwesterly winds associated with the Asian winter monsoon, which also cause downwelling along the southern Sumatra and Java coasts (Figure 9i). These thermocline signals apparently suppress coastal upwelling, warming SST in the eastern equatorial basin and along Sumatra and Java (Figure 9g), contributing to the rapid termination of the 1994 dipole in December. Interannual thermocline anomalies caused by seasonal wind stress are also positive in the southeastern basin during winter (Figure 9h), however, they are smaller than those associated with the seasonal cycle.

[47] These results indicate that summer/early fall monsoon winds in the southeastern tropical basin provide favorable conditions for IOZDM development, and that fall equatorial westerlies and northwesterly winter monsoon winds may have made an important contribution to the termination of the 1994 IOZDM event.

3.3. Effects of the Seasonal Cycle on the 1997 IOZDM

[48] The 1997 IOZDM (Figure 1 (right)) was an unusually strong event, characterized by an eastern antinode that peaked in November–December and a western antinode that peaked later, in January–February 1998. This was well simulated by our model (Figure 10 (left)), excepting a phase delay of the peak and termination (see Figure 6) and some exaggeration of the eastern antinode magnitude in our model, as discussed in section 3.1 above. The interannual SSTA patterns caused by seasonal atmospheric forcing for this event (Figures 10 (right) and 11) are qualitatively similar to the patterns in 1994. However, in 1997/1998, the magnitudes of responses in the eastern antinode tend to be larger than in 1994, in addition to other differences. In the following, we focus primarily on how and why the SSTA responses to seasonal forcings in 1997/1998 differ from those in 1994.

3.3.1. SSTA Response to Total Seasonal Forcing

[49] In 1997, fall warming of interannual SSTA by total seasonal forcing along the equator is notably stronger than in 1994 and extends across a large area in the central and eastern basin (Figures 10d and 11a). Negative SSTA associated with the IOZDM within the boxed region at the equator is reduced by $\sim$1–1.5 °C on average because of the seasonal cycle. Note that from November to January, the warming maximum in the central basin propagates westward to about 65°E. Time-longitude plots [*Halkides*, 2005] show this westward propagation clearly. However, in results from an analogous experiment performed using a fully forced version of the 4-1/2 layer ocean model with identical wind stress forcing and prescribed near-surface air temperature and specific humidity, this westward propagation disappears and the magnitude of warming in the central basin is smaller by $\sim$1°C [*Halkides*, 2005], which is more consistent with the magnitude of observed SST. (In the fully forced model experiments discussed by *Halkides* [2005], air temperature and specific humidity fields were created using COADS climatology data and interannual anomalies from the NCEP-NCAR Reanalysis.) In the present results, air heated and moistened by warm SSTA induced by the seasonal cycle is likely advected westward by interannual easterlies and feeds back onto SST. Consequently, seasonal forcing also amplifies the warm western antinode associated with this event during its peak in January–February 1998 (Figure 10f). The degree of feedback, however, is likely exaggerated, because the fully forced version produced somewhat more realistic SSTA.

[50] Summer–fall cooling of interannual SSTA by seasonal forcing off southern Sumatra and Java is comparable in 1997 and 1994 (Figures 10b, 10d, and 11c). However, in December 1997 through spring of 1998, SSTA near southern Sumatra-Java exhibits significant warming due to seasonal forcing. This warming is much larger than that present during the 1994 IOZDM termination period (compare Figures 11c to 8c). It will be shown that in 1997/1998

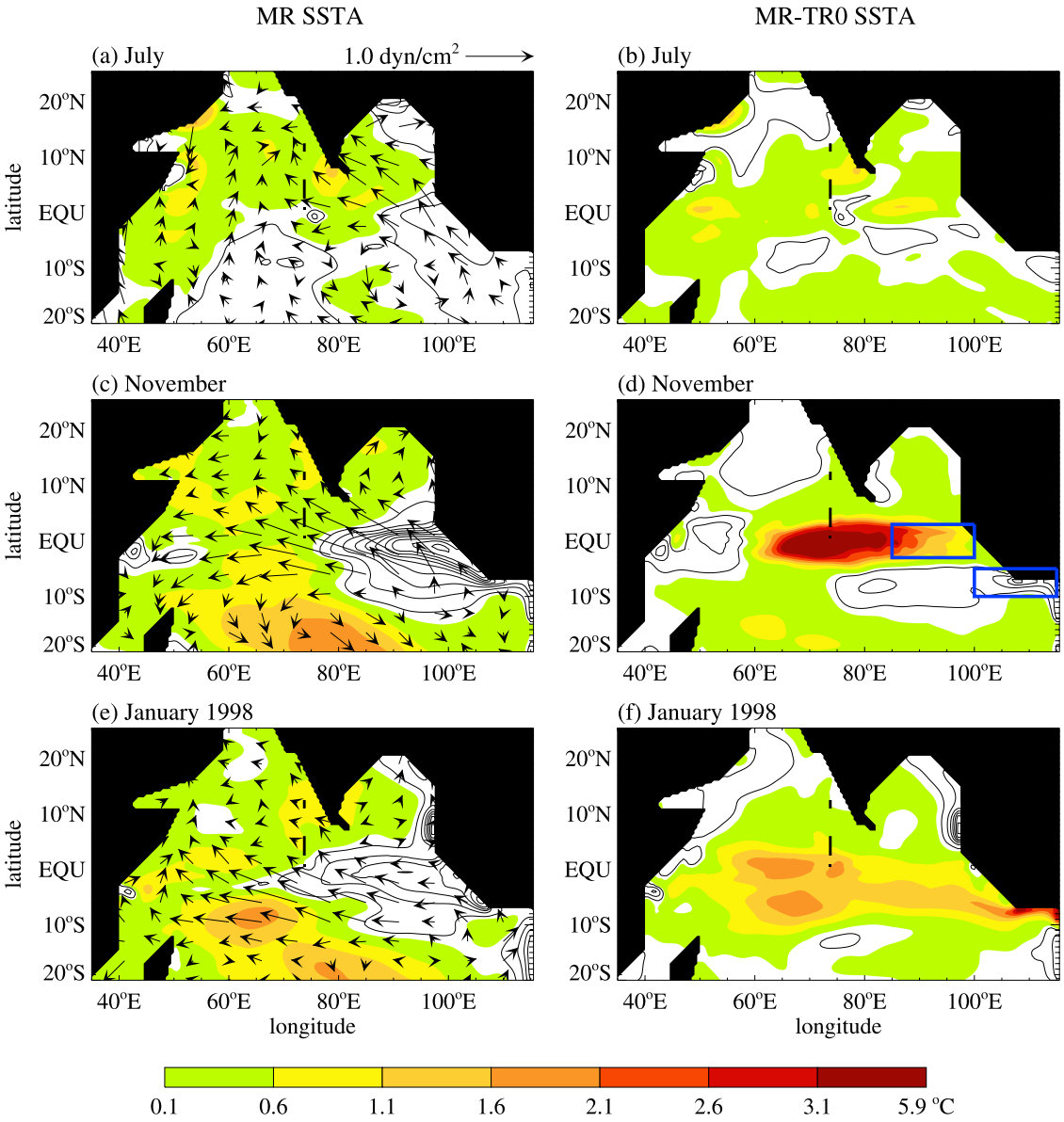

Figure 10. (left) Interannual MR SSTA with interannual FSU wind stress anomalies and (right) MR minus TR0 SSTA for select months during the 1997/1998 IOZDM. Positive anomalies are colored; negative anomalies are shown with line contours at an interval of 0.5 °C. Wind vectors are in dyn/cm^2. Difference panels in the right-hand column show the interannual SSTA response to total seasonal atmospheric forcing.

conditions in our model are such that the eastern antinode is significantly more sensitive to seasonal forcing than in 1994, likely due to the unusually strong interannual easterlies, shallow thermocline and thin mixed layer during the 1997/1998 IOZDM event (see below). Even though the seasonal cycle has a larger influence on the 1997 event, warming of the eastern antinode by the seasonal equatorial westerlies during fall and by the winter monsoon is insufficient to fully overcome the negative SSTA associated with this event (Figures 10c–10f). Consequently, the seasonal equatorial westerly winds only act to weaken the event, not to terminate it. This is in contrast with 1994, as warming of SSTA in the eastern equatorial region by the seasonal westerlies during October–November is concurrent with, and instrumental to the early termination of that event (Figures 7 and 8).

3.3.2. Processes

[51] Below, we examine the most important processes through which the seasonal cycle modifies the 1997/1998 IOZDM. The interannual SSTA induced by seasonal wind stress, wind speed and insolation in the eastern equatorial basin and near Java during the 1997/1998 IOZDM can be compared in Figures 11b and 11d, respectively.

[52] It is shown above that, as in 1994, the seasonal cycle tends to warm the eastern equatorial region during fall and winter 1997, especially in November (Figure 11a). Interestingly, while wind stress is still an important factor for this warming during September–November, SSTA caused by

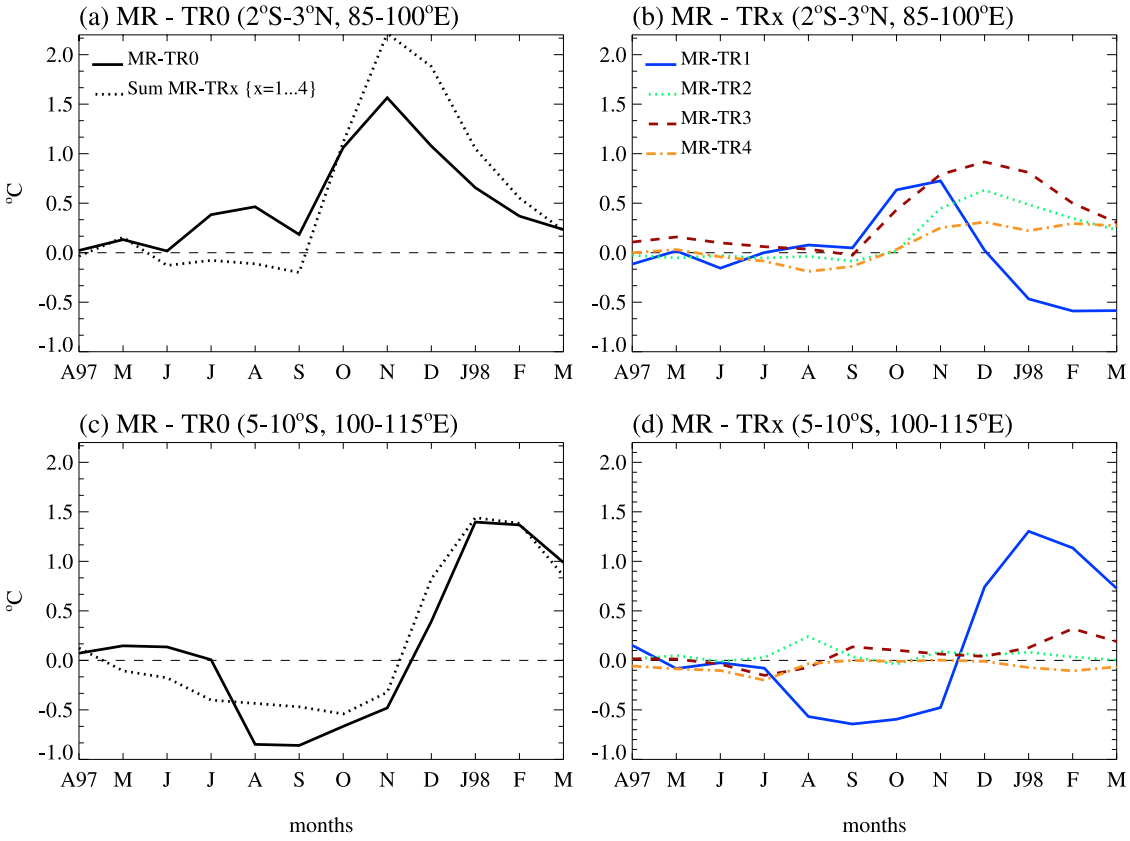

Figure 11. The mean SSTA responses (MR-TRx) (left) to total seasonal forcing and (right) to isolated seasonal forcings from April 1997 through March 1998 in two subregions of the eastern antinode: along the equator (2°S–3°N, 85°–100°E) and in the southern Sumatra-Java upwelling region (5°–10°S, 100°–115°E). Figures 11a and 11c also include the summation of the isolated responses for comparison to the MR-TR0 indices. Index boxes are shown in Figures 7d and 10d.

surface heat flux and entrainment due to seasonal wind speed have comparable amplitudes, and together, they dominate the effects of seasonal wind stress during November–December 1997 (Figures 11a and 11b). This is in contrast to 1994, when seasonal wind stress forcing dominates in this region until December and the responses to seasonal wind speed are much smaller. Seasonal insolation associated with austral summer also acts to warm SSTA in the eastern equatorial basin from November 1997 to spring 1998, but while this response is larger than that during the 1994 event (dash-dotted lines in Figures 8b and 11b), it is still small compared to the effects of seasonal wind speed and wind stress. Near southern Sumatra and Java, on the other hand, the 1997 interannual SSTA induced by seasonal forcing is dominated by wind stress (solid line in Figure 11d), as in 1994. Causes for the clear differences between the 1997 and 1994 events are discussed below.

3.3.2.1. SSTA Response to Seasonal Wind Stress

[53] Figure 12 shows the interannual MR-TR1 SSTA (left), interannual MR-TR1 thermocline anomaly (middle), and the seasonal cycle of the MR-TR1 thermocline variability (right), representing the response of the system to seasonal wind stress forcing during the 1997/1998 IOZDM. Similar to 1994, SSTA along the southern Sumatra-Java coasts exhibits cooling in summer (Figure 12a), because seasonal southeasterlies associated with the Asian summer monsoon reinforce the southeasterly wind anomalies associated with the IOZDM (Figures 2a and 1b), raising the interannual thermocline south of Java (Figure 12b). This condition favors IOZDM initiation and development. During August–October, the seasonal cycle of the thermocline (refer back to Figure 9f) also exhibits shoaling in the southeastern basin, which further enhances upwelling cooling.

[54] In contrast to fall–winter 1994, when seasonal wind stress produces a weakly positive anomaly in the interannual thermocline in the eastern equatorial ocean, seasonal wind stress during fall–winter 1997 produces a significant negative anomaly in the interannual thermocline in this region (compare Figures 12e, 12h, 9e, and 9h). This is likely because the stronger southeasterly wind anomalies associated with the 1997 IOZDM produce a much shallower thermocline (and thinner h_1) in the eastern equatorial ocean and along the coasts of Sumatra-Java (Figure 13). Under these conditions, the sensitivity of the thermocline itself to wind stress forcing is enhanced, such that the seasonal southeasterly monsoon winds produce a larger shoaling response in the interannual thermocline anomaly in 1997 than in 1994. Consequently, these negative interannual thermocline anomalies act to cool SSTA near the

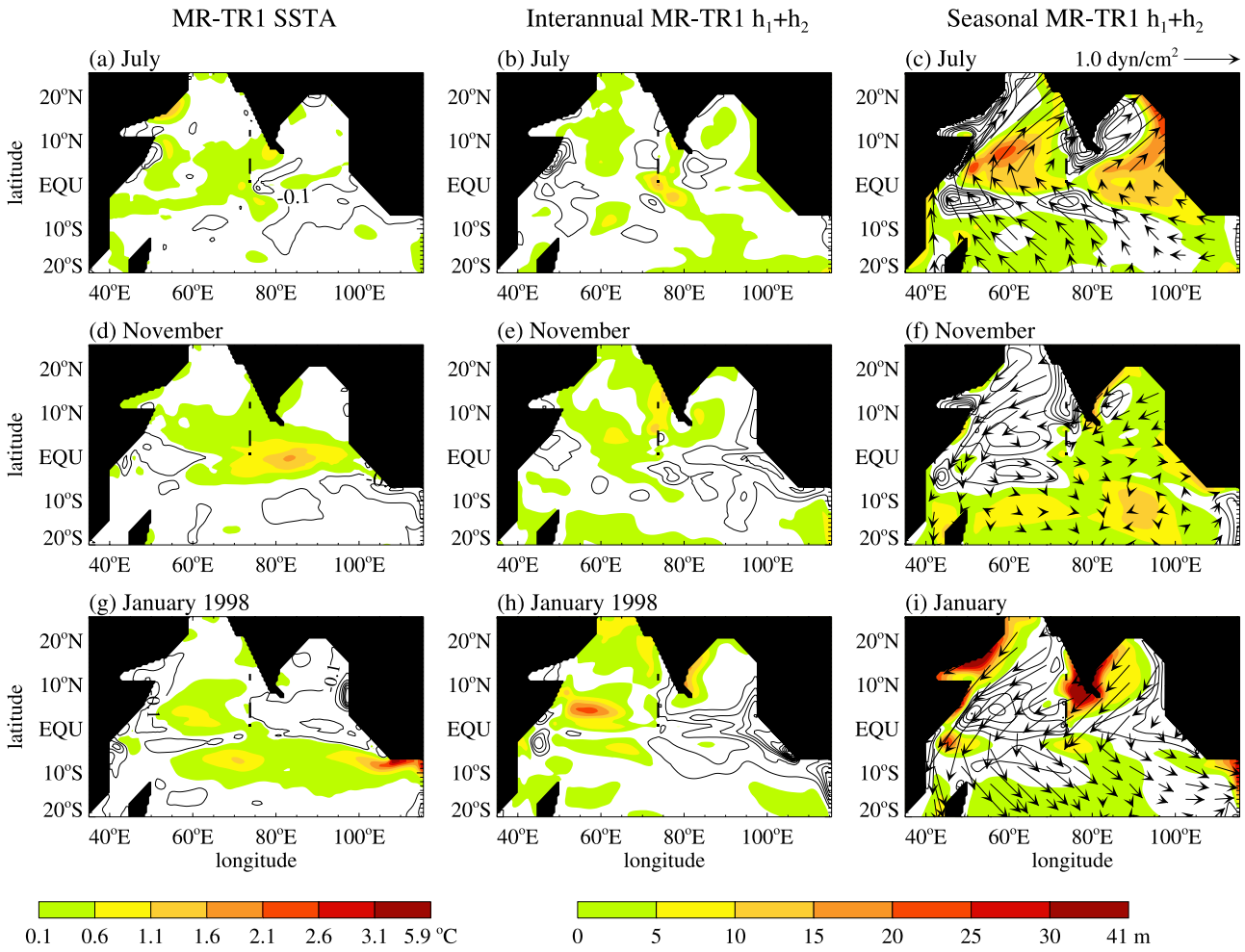

Figure 12. (left) Interannual MR minus TR1 SSTA for select months during the 1997/1998 IOZDM. This represents the effect of seasonal wind stress on interannual SSTA variability. (meddle) Interannual MR minus TR1 thermocline depth in meters. (right) Seasonal cycle of MR minus TR1 thermocline depth. Vectors show seasonal FSU wind stress in dyn/cm^2, the signal that was removed from the TR1 forcing. Positive anomalies are colored; negative anomalies are shown with line contours. Different months are shown than in Figure 9, although the seasonal cycle of the MR-TR1 thermocline depth is the same for all years.

Sumatra-Java coasts during the 1997 IOZDM fall peak and in the eastern equatorial region in January (Figures 12d–12i). This is in stark contrast to 1994, when this effect is weak and dominated by rectification in the eastern equatorial basin due to the fall equatorial westerlies during the IOZDM peak (Figures 9d–9f, section 3.2).

[55] Along the equator, seasonal westerlies during fall do cause deepening in the seasonal cycle of the thermocline in the eastern basin (Figures 12f, 3, and 5). This reduces the upwelling associated with the 1997 IOZDM and causes positive SSTA in the central and eastern equatorial region (Figure 12d). This deepening subsequently propagates to the south along the Sumatra-Java coasts, producing a strong positive SSTA response south of Java in January (Figures 12g and 12i). Concurrently, the seasonal northwesterly winds associated with the Asian winter monsoon act to deepen the thermocline and further reduce upwelling along the coasts of Sumatra-Java, contributing to this warming of SSTA (Figures 12g, 12i, and 2). A similar effect occurs during the 1994 IOZDM termination.

[56] The fact that the interannual thermocline response to seasonal wind stress exhibits shoaling during fall–winter 1997, instead of deepening as in 1994, may explain why the seasonally deepened thermocline associated with the fall Wyrtki jet only weakens the 1997 IOZDM, but does not terminate it. As discussed in section 3.2, this effect does contribute significantly to the 1994 IOZDM termination. Additionally, the positive SSTA induced by the seasonal wind stress near Java in January 1998 extends far to the west (Figure 12g). This is associated with interannual northwestward currents (not shown) that occur in this region during the strong IOZDM [*Saji et al.*, 1999; *Murtugudde et al.*, 2000] and advect the warm SSTA toward the interior basin [*Murtugudde et al.*, 2000].

[57] In January, the SSTA response to seasonal wind stress in the eastern equatorial basin is negative. This results

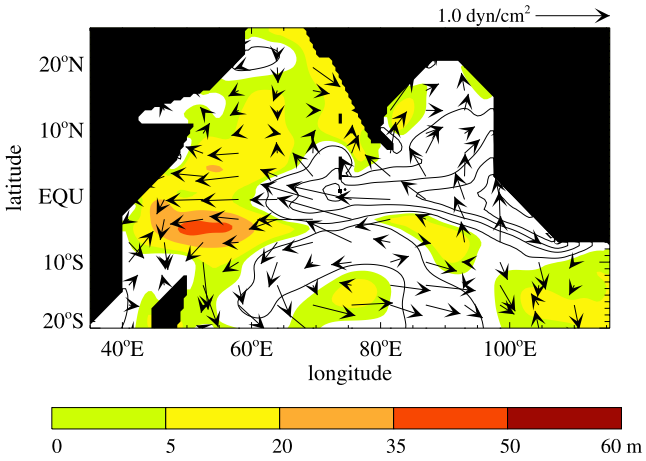

Figure 13. November 1997 minus November 1994 thermocline depth, with 1997 minus 1994 FSU wind stress difference vectors superimposed on the contours. Positive thermocline difference values are colored; negative values are shown with line contours, beginning at 5 m and continuing at intervals of 15 m. Wind stress difference vectors are in dyn/cm^2.

from both the negative interannual thermocline anomaly and seasonal shoaling of the thermocline in this region (Figures 12g–12i). Shoaling along the equator in January is most likely associated with seasonal weakening of the equatorial westerlies (Figure 3a) during the Asian winter monsoon. These signals act to enhance rather than reduce the eastern IOZDM antinode. This may explain why the eastern antinode associated with the 1997/1998 IOZDM does not decay until January 1998 (Figures 10e and 6).

[58] Note that Figure 13 shows that the thermocline in the western basin between the equator and 10°S is significantly deeper in fall 1997 than in 1994. This elongated depression can be associated with westward downwelling Rossby waves driven by the unusually strong interannual easterlies in this year, to which *Webster et al.* [1999] partly attributed the late peak and prolonged duration of the 1997/1998 western antinode.

3.3.2.2. SSTA Response to Seasonal Wind Speed

[59] Figures 14a and 14c (Figures 14b and 14d) show the interannual SSTA due to modulation of entrainment cooling (surface turbulent heat fluxes) by seasonal wind speed during November 1997 and January 1998. These months coincide with the peak and termination periods of the negative SSTA in the eastern antinode region. In November–December 1997, there is notable warming of interannual

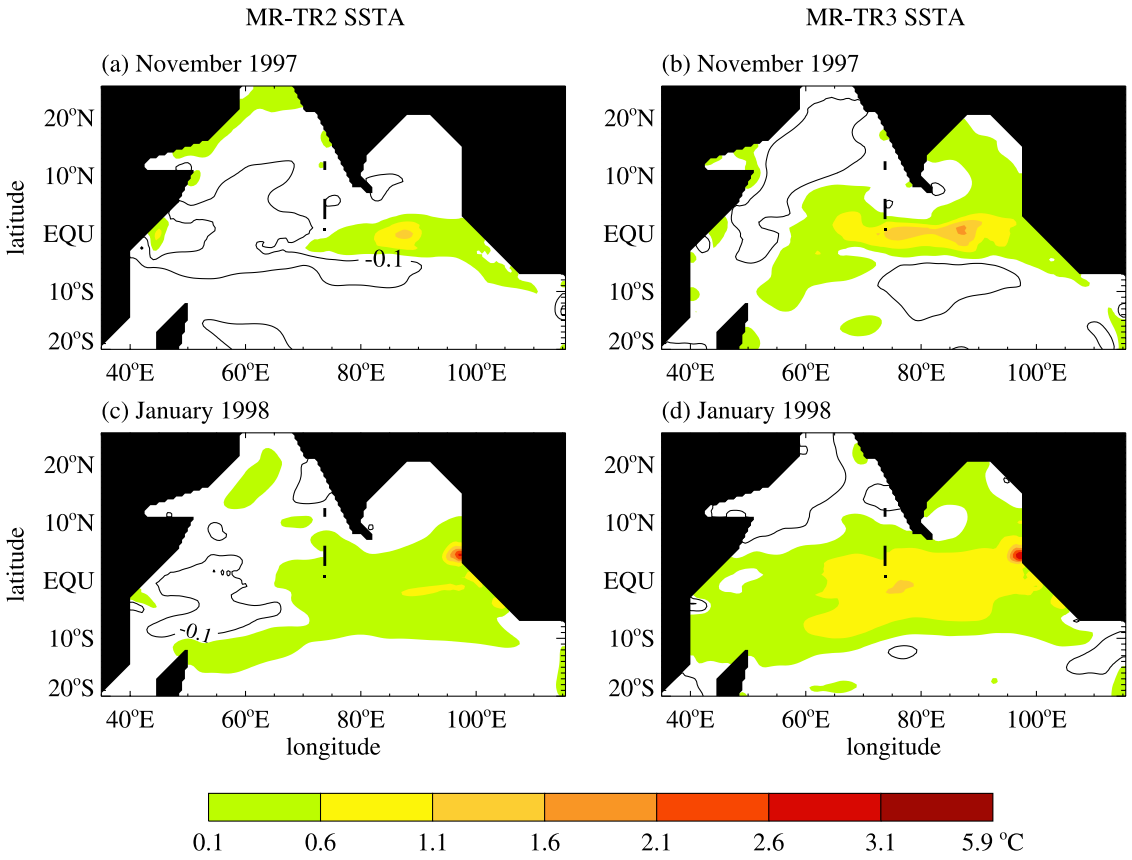

Figure 14. (left) Interannual MR minus TR2 SSTA during November 1997 (when the eastern IOZDM antinode peaks) and January 1998 (when the eastern antinode decays). This represents the effect of seasonal wind speed-driven entrainment on interannual SSTA. (right) Interannual MR minus TR3 SSTA during the same months. This estimates the effects of surface turbulent heat fluxes caused by seasonal wind speed. Units are °C. Positive anomalies are colored; negative anomalies are shown with line contours.

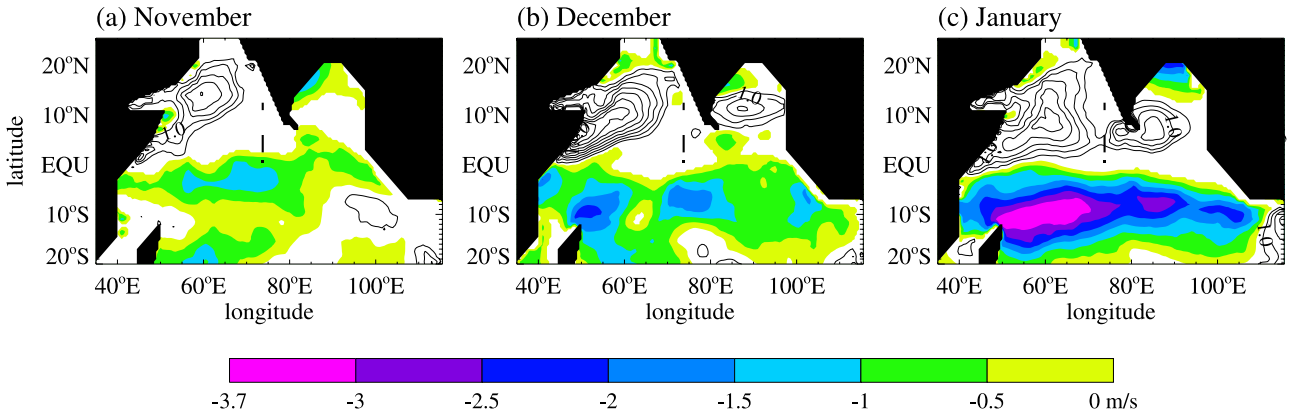

Figure 15. The difference between wind speed used in the AML model component for the MR (which retains the seasonal cycle) and TR3 (which excludes the seasonal cycle) for (a) November 1997, (b) December 1997, and (c) January 1998. Negative values indicate reduced wind speed due to the seasonal cycle and are colored; positive values indicate enhanced wind speed by the seasonal cycle and are shown by line contours. Units are m/s.

SSTA across the central and eastern equatorial basin due to reductions in both entrainment cooling (Figures 14a, 14c, and 11b) and surface heat loss (Figures 14b, 14d, and 11b) caused by seasonal wind speed. This occurs as follows. Unlike the 1994 event which peaks in October of that year, the 1997 eastern antinode begins to peak in November, when seasonal equatorial westerlies reach their maximum amplitude (Figure 3a). Competition between November westerlies and interannual easterlies (Figure 10c) results in a reduction of net wind speed along the equator (Figure 15a). This in turn causes reductions in entrainment cooling and surface heat loss in the eastern basin, via the processes discussed in section 2.4. The resultant warming continues in the eastern basin through spring 1998 (Figure 11b).

[60] During January in the southern basin, seasonal northwesterly winds associated with the winter monsoon also weaken southeasterlies associated with the IOZDM (Figures 15b and 15c). Ensuing reductions of entrainment cooling and surface heat loss produce positive SSTA in the southern basin (Figures 14c and 14d).

[61] These results suggest that reduced entrainment cooling and surface heat loss due to seasonal wind speed both work to mitigate cold SSTA in the eastern antinode region during the peak and termination periods of the 1997/1998 IOZDM and thus aid decay of this event. Similar, but much weaker responses to seasonal wind speed occur in 1994 (not shown). However, the effect is greater in 1997 because of the much shallower thermocline and correspondingly thinner mixed layer in the eastern basin, as suggested by *Murtugudde et al.* [2000] (Figure 13). Additionally, during the 1997 event, warming associated with reduced surface heat loss during the winter monsoon also persists in the central and southwestern basin through spring 1998 [*Halkides*, 2005] (Figure 14d). Thus seasonal wind modulation of surface heat flux plays a role in delaying the decay of the warm western antinode in 1997/1998.

4. Summary and Discussion

[62] This study demonstrates the importance of seasonal atmospheric forcing to the development, magnitude and termination of interannual SSTA associated with IOZDM events. A nonlinear 4-1/2 layer model of the IO, coupled to an advective atmospheric mixed layer model through SST feedback to air temperature and humidity, was used to estimate contributions of physical processes through which the seasonal cycle of atmospheric forcing modulates interannual SSTA during the strong 1994 and 1997 IOZDM events. These processes include: (1) thermocline variability induced by seasonal wind stress; (2) modulation of entrainment cooling by seasonal wind speed; (3) modulation of surface turbulent heat fluxes by seasonal wind speed; (4) surface heating by seasonal insolation. The effect of seasonal cloud variability on outgoing long wave radiation was found insignificant to modulation of the IOZDM. Our primary results are summarized below.

[63] In June–July of both 1994 and 1997, dynamic forcing by seasonal southeasterlies associated with the Asian summer monsoon, aids initiation of negative SSTA in the southern portion of the eastern IOZDM antinode. Cooling near Java persists through both IOZDM peaks, strengthening both events.

[64] Seasonal equatorial westerlies during fall, which depress the thermocline in the eastern IO and drive the fall Wyrtki jet, reduce negative SSTA in the eastern equatorial basin during both the 1994 and 1997 eastern IOZDM antinode peak periods. The deepened thermocline subsequently propagates south along the coasts of Sumatra and Java via coastal Kelvin waves, reducing cold SSTA in the southeastern basin. This process appears to make an important contribution to the 1994 IOZDM termination. Northwesterly winds associated with the Asian winter monsoon during both 1994 and 1997 cause downwelling near the southern Sumatra and Java coasts, which also contributes to eastern antinode termination.

[65] Interestingly, fall equatorial westerlies cause notably stronger warming in 1997 than in 1994, yet only weaken the 1997 IOZDM, failing to terminate it. This is because during the extreme 1997 event, southeasterly wind anomalies associated with the IOZDM are much stronger and the thermocline in the eastern tropical basin is much shallower than in 1994. Two effects ensue: (1) warming in the

equatorial basin during fall 1997 is strong, as SST is very sensitive to thermocline variability due to the extremely shallow thermocline, and (2) under these conditions, seasonal southeasterlies near Sumatra-Java associated with the summer monsoon produce large negative anomalies in the interannual thermocline signal during late summer and fall. During winter, shoaling also occurs in the seasonal cycle along the equator when the equatorial westerlies die down during the winter monsoon. The shallow thermocline in the equatorial region produces negative SSTA during December–January, which enhances rather than reduces the 1997 eastern antinode, despite the strong warming caused by the fall equatorial westerlies and subsequent reduction of upwelling along southern Sumatra-Java in winter via CKWs.

[66] In 1997, low wind speeds in the eastern equatorial region, due to reduction of interannual easterlies by the seasonal fall westerlies, decrease surface turbulent heat loss and entrainment cooling. Enhanced by an unusually thin mixed layer, these effects contribute significantly to warming of the eastern antinode. Reduction of the southeasterly trades during the winter monsoon also aids termination of cold SSTA along Sumatra-Java through these same processes. Analogous effects occur in fall–winter 1994 [*Halkides*, 2005], but are very mild.

[67] Seasonal solar heating during austral summer, enhanced by the anomalously thin mixed layer in the southeastern IO, contributes to the 1997/1998 eastern antinode termination, but is much less significant than warming caused by seasonal wind stress and wind speed effects.

[68] This work highlights additional issues to be addressed in the future. The importance of air-sea interaction in IOZDM evolution is evident from the amplification of SSTA responses to seasonal forcing when SST feedback to air temperature and humidity is added to the 4-1/2 layer ocean. This model, however, has no ocean feedback to winds. The fact that, even with removal of all seasonal forcing, IOZDM events are still phase-locked to the seasonal cycle indicates seasonal effects may remain in the observed interannual forcings. Variations on these experiments using a fully coupled model should be performed. Other authors have studied the roles of the Tropical Biennial Oscillation [*Loschnigg et al.*, 2003] and of intraseasonal climate variability [*Han et al.*, 2006; *Rao and Yamagata*, 2004] in IOZDM development and phase locking. Interplay of phenomena of differing timescales that contribute to IOZDM development should be examined to improve prediction of IOZDM behavior.

[69] **Acknowledgments.** Our appreciation goes to R. Seager at Columbia University for use of the atmospheric mixed layer model code, and to Y-C. Zhang and W. Russow at NASA for providing radiation flux data. We thank both anonymous reviewers for their careful and thoughtful comments. Daria J. Halkides and Weiqing Han were supported by NSF OCE-0136836 and NSF OCE-0452917, and Peter J. Webster was supported by NSF ATM-0531771.

References

Annamalai, H., R. Murtugudde, J. T. Potemra, S. P. Xie, and B. Wang (2003), Coupled dynamics in the Indian Ocean: Externally or internally forced?, *Deep Sea Res., Part I*, *50*, 2305–2330.

Ashok, K., Z. Guan, and T. Yamagata (2001), Impact of the Indian Ocean Dipole on the decadal relationship between the Indian monsoon rainfall and ENSO, *Geophys. Res. Lett.*, *28*, 4499–4502.

Carton, J. A., G. Chepurin, and X. Cao (2000), A simple ocean data assimilation analysis of the global upper ocean 1950–95. part I: Methodology, *J. Phys. Oceanogr.*, *30*, 294–309.

Chambers, D. P., B. D. Tapley, and R. H. Stewart (1999), Anomalous warming in the Indian Ocean coincident with El Nino, *J. Geophys. Res.*, *104*, 3035–3048.

Clark, C. O., J. E. Cole, and P. J. Webster (2000), Indian Ocean SST and Indian summer rainfall: Predictive relationships and their decadal variability, *J. Clim.*, *13*, 2503–2519.

Clark, C., P. Webster, and J. Cole (2003), Interdecadal variability of the relationship between the Indian Ocean Zonal Mode and east African coastal rainfall anomalies, *J. Clim.*, *16*, 548–554.

Clarke, A. J., and X. Liu (1993), Observations and dynamics of semiannual and annual sea levels near the eastern equatorial Indian Ocean boundary, *J. Phys. Oceanogr.*, *23*, 386–399.

Halkides, D. J. (2005), The effects of the seasonal cycle on interannual SST variability in the Indian Ocean, Ph.D. thesis, Dep. of Atmos. and Oceanic Sci., Univ. of Colo., Boulder.

Han, W. (1999), Influence of salinity on dynamics, thermodynamics and mixed layer physics in the Indian Ocean, Ph.D. thesis, Nova Southeastern Univ., Fort Lauderdale-Davie, Fla.

Han, W., and J. P. McCreary (2001), Modeling salinity distribution in the Indian Ocean, *J. Geophys. Res.*, *106*, 859–877.

Han, W., and P. J. Webster (2002), Forcing mechanisms of sea-level interannual variability in the Bay of Bengal, *J. Phys. Oceanogr.*, *32*, 216–239.

Han, W., J. P. McCreary, D. L. T. Anderson, and A. J. Mariano (1999), On the dynamics of the eastward surface jets in the equatorial Indian Ocean, *J. Phys. Oceanogr.*, *29*, 2191–2209.

Han, W., P. J. Webster, R. Lukas, P. Hacker, and A. Hu (2004), Impact of atmospheric intraseasonal variability in the Indian Ocean: Low-frequency rectification in equatorial surface current and transport, *J. Phys. Oceanogr.*, *34*, 1350–1372.

Han, W., T. Shinoda, L. Fu, and J. P. McCreary (2006), Impact of atmospheric intraseasonal oscillations on the Indian Ocean dipole during the 1990s, *J. Phys. Oceanogr.*, *36*(4), 670–690.

Jensen, T. G. (1993), Equatorial variability and resonance in a wind-driven Indian Ocean model, *J. Geophys. Res.*, *98*, 22,533–22,552.

Kapala, A., K. Born, and H. Flohn (1994), Monsoon anomaly or an El Nino in the equatorial Indian Ocean?: Catastrophic rains in East Africa and their teleconnections, paper presented at International Conference on Monsoon Variability and Prediction, World Meteorol. Org., Trieste, Italy, 3–13 May.

Kindle, J. C., and J. D. Thompson (1989), The 26–50 days oscillation in the western Indian Ocean: Model results, *J. Geophys. Res.*, *94*, 4721–4736.

Kraus, E. B., and J. S. Turner (1967), A one-dimensional model of the seasonal thermocline II: The general theory and its consequences, *Tellus*, *119*, 98–106.

Legler, D. M., I. M. Navon, and J. J. O'Brien (1989), Objective analysis of pseudostress over the Indian Ocean using a direct-minimization approach, *Mon. Weather Rev.*, *117*, 709–720.

Loschnigg, J., G. Meehl, P. J. Webster, J. Arblaster, and G. Compo (2003), The Asian monsoon, the tropical biennial oscillation, and the Indian Ocean Zonal Mode in the NCAR CSM, *J. Clim.*, *16*, 1617–1642.

Luther, M. E., and J. J. O'Brien (1985), A model of the seasonal circulation in the Arabian Sea forced by observed winds, *Prog. Oceanogr.*, *14*, 353–385.

Maghanani, V., B. Subrahmanyam, L. Xie, and J. Morrison (2003), Numerical simulation of seasonal and interannual Indian Ocean upper layer circulation using MICOM, *J. Geophys. Res.*, *108*(C7), 3240, doi:10.1029/2002JC001567.

Mariano, A. J., E. H. Ryan, B. D. Perkins, and S. Smithers (1995), The Mariano Global Surface Velocity Analysis 1.0, *USCG Rep. CG-D-3495*, 55 pp., U.S. Geodyn. Comm., Washington, D. C.

McCreary, J. P., and P. K. Kundu (1989), A numerical investigation of sea surface temperature variability in the Arabian Sea, *J. Geophys. Res.*, *94*, 16,097–16,114.

McCreary, J. P., P. K. Kundu, and R. L. Molinari (1993), A numerical investigation of dynamics, thermodynamics and mixed-layer processes in the Indian Ocean, *Prog. Oceanogr.*, *31*, 181–244.

Morel, A., and D. Antoine (1994), Heating rate within the upper ocean in relation to its bio-optical state, *J. Phys. Oceanogr.*, *24*, 1652–1665.

Murtugudde, R., R. Seager, and A. Busalacchi (1996), Simulation of the tropical oceans with an ocean GCM coupled to an atmospheric mixed layer model, *J. Clim.*, *9*, 1795–1815.

Murtugudde, R., S. Signorini, J. Christian, A. Busalacchi, and C. McClain (1999), Ocean color variability of the tropical Indo-Pacific basin observed by SeaWiFS during 1997–1998, *J. Geophys. Res.*, *104*, 18,351–18,366.

Murtugudde, R., J. P. McCreary, and A. J. Busalacchi (2000), Oceanic processes associated with anomalous events in the Indian Ocean with relevance to 1997–1998, *J. Geophys. Res.*, *105*, 3295–3306.

Rao, R. R., and R. Sivakumar (2000), Seasonal variability of near-surface thermal structure and heat budget of the mixed layer of the tropical Indian Ocean from a new global ocean temperature climatology, *J. Geophys. Res.*, *105*, 995–1015.

Rao, S. A., and T. Yamagata (2004), Abrupt termination of Indian Ocean dipole events in response to intraseasonal oscillations, *Geophys. Res. Lett.*, *31*, L19306, doi:10.1029/2004GL020842.

Reverdin, G. (1987), The upper equatorial Indian Ocean: The climatological seasonal cycle, *J. Phys. Oceanogr.*, *17*, 903–927.

Reverdin, G., D. L. Cadet, and D. Gutzler (1986), Interannual displacements of convection and surface circulation over the equatorial Indian Ocean, *Q. J. R. Meteorol. Soc.*, *112*, 43–67.

Saji, N. H., B. N. Goswami, P. N. Vinayachandran, and T. Yamagata (1999), A dipole mode in the tropical Indian Ocean, *Nature*, *401*, 360–363.

Schiller, A., and J. S. Godfrey (2003), Indian Ocean intraseasonal variability in an ocean general circulation model, *J. Clim.*, *16*, 21–39.

Schott, F., and J. P. McCreary Jr. (2001), The monsoon circulation of the Indian Ocean, *Prog. Oceanogr.*, *51*, 1–123.

Seager, R., M. B. Blumenthal, and Y. Kushnir (1995), An advective atmospheric mixed layer model for ocean modeling purposes: Global simulation of surface heat fluxes, *J. Clim.*, *8*, 1951–1964.

Senan, R., D. Sengupta, and B. N. Goswami (2003), Intraseasonal "monsoon jets" in the equatorial Indian Ocean, *Geophys. Res. Lett.*, *30*(14), 1750, doi:10.1029/2003GL017583.

Shinoda, T., and W. Han (2005), Influence of Indian Ocean dipole on atmospheric subseasonal variability, *J. Clim.*, *18*, 3891–3909.

Smith, T. M., and R. W. Reynolds (2003), Extended reconstruction of global sea surface temperatures based on COADS data (1854–1997), *J. Clim.*, *16*, 1495–1510.

Susanto, R. D., A. L. Gordon, and Q. N. Zheng (2001), Upwelling along the coasts of Java and Sumatra and its relation to ENSO, *Geophys. Res. Lett.*, *28*, 1599–1602.

Webster, P. J., A. M. Moore, J. P. Loschnigg, and R. R. Leben (1999), Coupled ocean-atmosphere dynamics in the Indian Ocean during 1997–98, *Lett. Nature*, *401*, 356–360.

Wijffels, S., and G. A. Meyers (2004), An intersection of oceanic wave guides: Variability in the Indonesian Throughflow region, *J. Phys. Oceanogr.*, *34*, 1232–1253.

Wyrtki, K. (1973), An equatorial jet in the Indian Ocean, *Science*, *181*, 262–264.

Xie, S. P., H. Annamalai, F. A. Schott, and J. P. McCreary (2002), Structure and mechanisms of south Indian Ocean climate variability, *J. Clim.*, *15*, 864–878.

Yu, L., and M. Rienecker (1999), Mechanisms for the Indian Ocean warming during the 1997–1998 El Niño, *Geophys. Res. Lett.*, *26*, 735–738.

Zhang, Y.-C., W. B. Rossow, A. A. Lacis, V. Oinas, and M. I. Mishchenko (2004), Calculation of radiative flux profiles from the surface to top-of-atmosphere based on ISCCP and other global datasets: Refinements of the radiative transfer model and the input data, *J. Geophys. Res.*, *109*, D19105, doi:10.1029/2003JD004457.

D. J. Halkides and W. Han, Department of Atmospheric and Oceanic Sciences, University of Colorado, Boulder, CO 80309, USA. (djh@halkides-beck.com; whan@enso.colorado.edu)

P. J. Webster, School of Earth and Atmospheric Sciences, Georgia Institute of Technology, Atlanta, GA 30332, USA.